

# Frequency stability control support from ReGen plants

Agreement no.: PSO ForskEl 12347  
Project Name: Ancillary Services from Renewable Power Plants  
Acronym: RePlan  
Duration: 2015 - 2018  
Co-ordinator: DTU Wind Energy

## Document information

Document name:	Frequency stability support from ReGen plants
Document number:	D3
Contributors:	Müfit Altin, Junjie Hu, Anca D. Hansen
Document type:	Report
Date:	August 2017
WP:	3

## Content

Preface.....	4
1 Scope of document.....	5
2 Identification of frequency stability challenges .....	5
2.1 Background.....	5
2.2 Future challenges .....	6
3 Frequency control capabilities of ReGen Plants.....	8
3.1 Technical capabilities of WPPs .....	8
3.2 Technical capabilities of PVPs.....	9
3.3 Strengths and Limitations of ReGen Plants for Frequency Control.....	9
4 Fast Frequency Response .....	10
4.1 Motivation .....	11
4.1.1 Need for frequency support coordination from WPPs in island power system.....	11
4.1.2 Need for frequency support coordination from WPPs in large scale power system .....	13
4.2 Optimization of Aggregated FFR from WPPs.....	16
4.3 Optimization of Coordinated FFR from WPPs .....	21
4.4 Analysis of WT’s FFR Performance .....	27
5 Frequency Restoration Reserve.....	29
<b>5.1 Frequency Restoration Reserve (FRR) Control Principle .....</b>	<b>29</b>
<b>5.2 System architecture and assumptions.....</b>	<b>31</b>
<b>5.3 Statistical control method .....</b>	<b>34</b>
5.3.1 Control performance index .....	34
5.3.2 Wind and PV power uncertainty modeling.....	34
5.3.3 Statistical online decision system.....	35
5.3.4 Aggregator real-time controller .....	37
<b>5.4 Case studies.....</b>	<b>38</b>
5.4.1 Two wind power plants.....	38
5.4.2 Three PV plants.....	43
<b>5.5 Discussion.....</b>	<b>46</b>
6 Summary.....	46
7 References .....	47

## **Preface**

This report is the outcome of WP3 as the deliverable in the project “Ancillary services from renewable power plants” (RePlan). RePlan is funded by the Danish TSO as POS project 2015 no. 12347, and is carried out in collaboration between DTU Wind Energy, DTU Elektro, Aalborg University Energy Technology, Aalborg University Wireless Communication Networks and Vestas Wind System A/S. DTU Wind Energy is manager of the project.

## 1 Scope of document

This deliverable report summarizes the results of work package 3 (Frequency support from ReGen plants), including the related models, methodologies, development of controls and study cases considered for both primary and secondary frequency control.

The overall objective of this work package is to improve the frequency control support from ReGen plants (with especially focus on wind power plants) by optimizing and coordinating the total support from ReGen plants.

## 2 Identification of frequency stability challenges

### 2.1 Background

High penetration levels of variable ReGen energy in modern power systems challenges the secure and reliable operation of these power systems. Wind turbines, which are the substantial nonsynchronous ReGen plants in power systems, do not inherently provide frequency responsive services as conventional generations traditionally do. An example of such support service is fast frequency response and emulated inertia in the short-term frequency stability. Unlike fixed speed wind turbines or conventional power plants, the most modern wind turbine technologies today, i.e. variable speed wind turbines (VSWTs), do not inherently contribute to the system inertia, as they are decoupled from the power system through power converter interfaces. This means that the higher levels of VSWTs without additional specific control, the lower the system inertia and the larger frequency deviations can get during imbalances between active power production and consumption.

TSOs have started to analyse their power systems and to improve their knowledge of the power system behavior related to the system inertia [1]. The study tries to determine the current level of system inertia and to make projection for the future renewable energy-dominated power systems. There can be control requirements for ReGen plants for certain operation of power systems with low inertia.

In UK, SMART frequency control project [2] started to investigate similar problems to support the frequency stability. In Figure 1, the proposal from GE is given to measure the frequency and control with distributed generation units. This project also aims to coordinate the generating units to improve the frequency and rotor angle stability of UK electricity network.

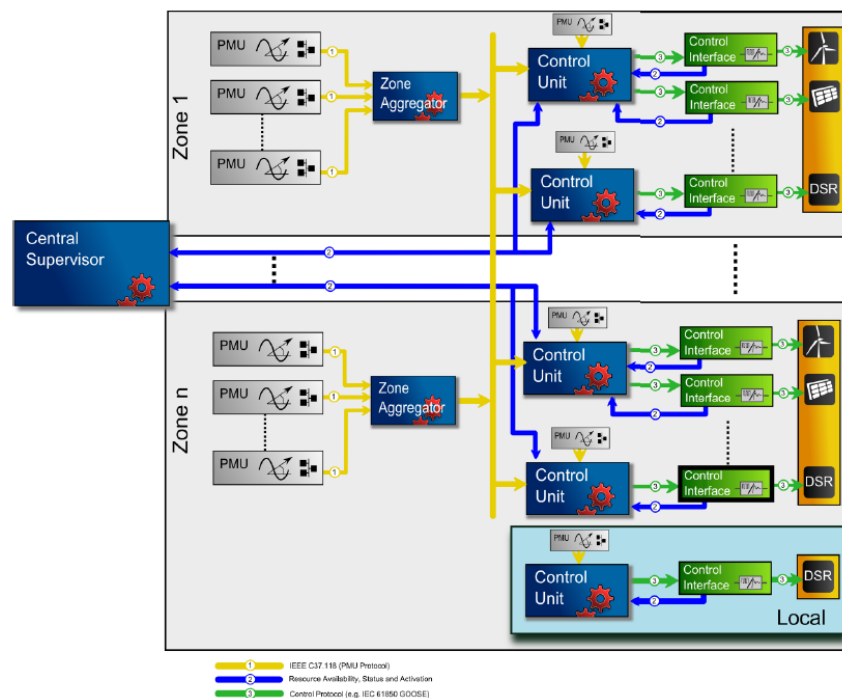


Figure 1. GE Proposal for SMART frequency control [2]

## 2.2 Future challenges

Future power systems face a range of challenges concerning their operability due to an increasing share of non-synchronous generation and a decreasing share of synchronous generation (the latter provides the main part of the system inertia today), which have direct impacts on the system inertia. Higher volumes of RES, phasing out of nuclear units, and high imports through HVDC connections all reduce inertia levels. It is therefore a crucial need to investigate the impact of such changes on system inertia and system operability and to seek ways to respond to new challenges.

Reduction of system inertia is one of the challenges faced by the future power system, implies a rise in the rate of change of frequency (ROCOF) which is a direct measure of the power system weakness with respect to withstanding sudden system imbalances after forced outages or system separations.

The challenges faced by the Nordic power system due to closure of thermal power plants, increased wind power penetration, decommissioning of nuclear power plants, increased interconnector capacity between the Nordic power system and others systems in the period leading up to 2025 are listed in the report [1]. These challenges should be seriously addressed otherwise there could be severe consequences. One of main challenges foreseen by the Nordic TSOs in the period leading up to 2025 lies in maintaining sufficient inertia in the system to guarantee operational security, since insufficient inertia would jeopardize the system stability in the event of a large unit trip. Higher volumes of RES, while decommissioning nuclear units, reduce inertia level and thus increase the rate of change of frequency, which is a direct measure of the power system weakness with respect to withstanding sudden system imbalances after forced outages or system separations. The power system inertia mainly derives from the kinetic energy stored in the rotors of the generators, which either is fed into or absorbed from the grid whenever there are frequency changes. Higher the inertia, slower the frequency decrease is, and thus longer time for the frequency containment reserves (FCR) to react.

According to [1], in 2025 the inertia, measured as kinetic energy, is estimated to be below the required volume of 120–145 GWs 1–19 per cent of the time depending on the climate year. Adding synthetic inertia to the system, adding rotating masses, such as synchronous condensers or setting minimum requirements for kinetic energy in the system are some of the possible solutions proposed in [1] for coping with low inertia. Future Nordic TOS’s projects target to anticipate, avoid and mitigate low system kinetic energy situations by estimating future kinetic energy levels, developing measures to handle low inertia situations and improving inertia estimation tools. There is an acute need for finding an estimate of the lowest amount of kinetic energy required in the system in order to satisfy the requirements for the lowest allowed instantaneous frequency. The kinetic energy in the system varies on a seasonal, and daily and weekly basis. The lowest kinetic energy values are observed during summer nights.

According to [6], in an interconnected power system, a very low value of system inertia is not considered to be critical for the normative 3000MW incident. However, this might have a significant impact if the interconnected power system suddenly splits, as it was the case of the Continental European power system November 4th 2006 event. Figure 2 illustrates that even if the system inertia i.e. the acceleration time constant of the network decreases down to  $T_N = 2.3$  s, the frequency deviation stays within the dynamically allowed range of  $\pm 800$ mHz.

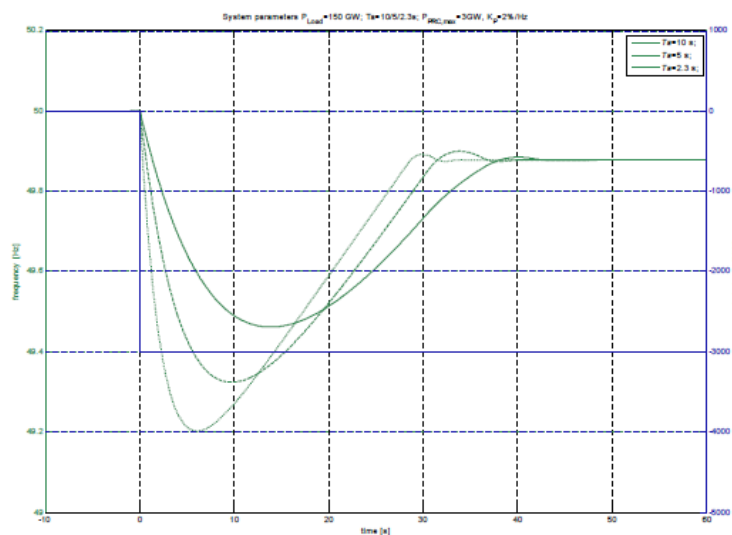


Figure 2. Frequency excursion for a reference incident of 3GW and different inertia (described as acceleration time constant  $T_N$ ) [6]

Today, the Continental European System with its current ability to withstand extreme frequency gradients can handle at the limit of stability a system imbalance ratio of 20%, corresponding to ROCOF ranging between 500mHz/s up to 1Hz/s [6]. A range of improvements with respect to generation and system protection devices capabilities is crucial in order to handle successfully the desired reference scenario of a maximum frequency gradient of 2Hz/s and an imbalance ratio of 40%.

### 3 Frequency control capabilities of ReGen Plants

In Deliverable 1.2, the technical feasibility of ancillary services is presented as an overview of the grid code requirements, future recommendations, technical and economic considerations. These inputs are exploited in this section and furthermore the details are presented in terms of control performance.

#### 3.1 Technical capabilities of WPPs

Variable speed wind turbines, which are the Type 3 (doubly-fed induction generator with partial scale converter) and the Type 4 (induction/synchronous generator with full scale converter) wind turbines, are designed to control the active power with a setpoint dependent on the wind speed. Without additional control implementation, wind power plants (WPPs), which are equipped with these WTs, cannot response to the frequency deviations during a power imbalance. In recent grid codes, synchronous generators are mainly responsible for controlling the power system frequency within the design limits. However, the requirements from WPPs for high shares of wind power scenarios in low inertia power systems might be increased in the future.

Requirements and capabilities of the generating units are specified in the grid codes as the frequency containment reserve (FCR, also known as primary control) and the frequency restoration reserve (FRR also known as secondary control). These reserve requirements are determined for a general range of performance specifications or control parameters. Each transmission system operator can adapt the parameters for each generating units in its area regarding the size and the technology of the synchronous generator and the market environment. Accordingly, separate requirements for WPPs have been published by TSOs and ENTSO-E [1], [5]. However, the synthetic inertia (or fast frequency response (FFR)) is not specified clearly, instead its control requirements and the performance parameters are leaved to the relevant TSO. The capabilities of WPPs are gathered from the literature based on the projects and publications. The requirements and the capabilities of WPPs are presented in the Table 1.

Table 1. Wind Power Plant Capabilities for Frequency Control

Feature	Grid Code Requirement	WPP Capability
Frequency ( $\Delta f$ & $df/dt$ ) Measurement [1]	80-100ms with $\pm 10$ mHz accuracy	Yes
FCR (Frequency Containment Reserve) [1]	$T_{start} < 2$ sec $T_{end} < 15$ sec Droop= 2%-12% (4% standard)	Yes
FRR (Frequency Restoration Reserve)	Pre-qualification test required, control error should be less than 1% for the whole testing period. [38]	Yes
FFR (Fast Frequency Response/ Synthetic Inertia) [1],[5],[6]	$T_{activation} < \text{a few } 100$ ms $T_{delivery} = 10$ s with $T_{delay} < 2$ s $H_{emulated inertia} = 3.5$ s for 10 s	Yes

### 3.2 Technical capabilities of PVPs

PV plants (PVPs) are required to have the same frequency control dynamics as WPPs mentioned in the Table 2 [4], [5].

**Table 2. PV Plant Capabilities for Frequency Control**

Feature	Grid Code Requirement	PVP Capability
Frequency ( $\Delta f$ & $df/dt$ ) Measurement [4]	80-100ms with $\pm 10$ mHz accuracy	Yes
FCR (Frequency Containment Reserve) [4]	$T_{start} < 2$ sec $T_{end} < 15$ sec Droop= 2%-12% (4% standard)	Yes
FRR (Frequency Restoration Reserve)	Pre-qualification test required, control error should be less than 1% for the whole testing period. [38]	Yes

### 3.3 Strengths and Limitations of ReGen Plants for Frequency Control

In order to present the capabilities of ReGen plants for frequency control, an analysis of their strengths, weaknesses, opportunities and threats (SWOT) is presented in Table 3.

**Table 3. Frequency control capabilities from ReGen – SWOT analysis.**

Category	Wind Power Plants	Photovoltaic Power Plants
Strengths	<ul style="list-style-type: none"> <li>Frequency control performance considering the settling time is faster than the conventional power plants.</li> <li>Wind turbine's kinetic energy can be employed in FFR.</li> </ul>	<ul style="list-style-type: none"> <li>Frequency control performance considering the settling time is faster than the conventional power plants.</li> </ul>
Weaknesses	<ul style="list-style-type: none"> <li>When wind turbine's kinetic energy is used, depending on the wind speed, there can be reduced active power output at the recovery period [39].</li> <li>Frequency measurement and rate of change of frequency estimation dynamics are challenging.</li> </ul>	<ul style="list-style-type: none"> <li>Reserve power is required.</li> <li>Frequency measurement and rate of change of frequency estimation dynamics are challenging.</li> </ul>
Opportunities	<ul style="list-style-type: none"> <li>Coordination between wind turbines or wind power plants can be applied to reduce the above mentioned weakness and to improve the overall response.</li> <li>Wind turbine based and power system based studies are required to explore the capabilities and to recommend inputs to the future grid codes.</li> </ul>	<ul style="list-style-type: none"> <li>Together with energy storage, the coordinated action can support the frequency control.</li> </ul>

	<ul style="list-style-type: none"> <li>• Together with energy storage, the coordinated action can support the frequency control.</li> </ul>	
Threats	<ul style="list-style-type: none"> <li>• Allocation together with rotor angle stability and power oscillation damping support can be complicated.</li> <li>• Wrong activation of the FFR can endanger the frequency stability and reserve.</li> <li>• If the forecast is employed in the control algorithms, error of the forecast should be compensated.</li> <li>• Communication and measurement delays should be crucial for fast and reliable responses.</li> </ul>	<ul style="list-style-type: none"> <li>• If the forecast is employed in the control or decision algorithms, error of the forecast should be compensated.</li> <li>• Communication and measurement delays should be crucial for fast and reliable responses.</li> </ul>

#### 4 Fast Frequency Response

Several research studies have been carried out towards development of new control features, like Fast Frequency Response (FFR). For instance, Hydro-Quebec and Electricity Reliability Council of Texas (ERCOT) have analyzed the possibility to request emulated inertia/synthetic inertial response to be incorporated into future WPPs [1-4], while the TSO in Great Britain (NGET) has investigated the possibility to include the fast frequency control into their grid code requirement [11].

The FFR of WPPs refers to the short-term additional active power contribution that can temporarily be released by using the stored kinetic energy in the rotating mass of variable speed WTs. FFR delivered by WPPs might become attractive in the context of large displacement of conventional power plants by WPPs in the future. According to [7], [8] the consideration of FFR as ancillary services should proceed cautiously and with focus on functional systematic needs, as WPPs' contribution is temporary being dependent on wind conditions, mechanical/electrical limitations, control strategies and availability of WPPs. Unlike the inherent response of synchronous generators (SGs), the capability of WPPs of injecting short-term additional active power into the grid is strongly dependent on wind speed conditions, mechanical/electrical limitation and proprietary control strategy of the turbines. In the optimization studies, which are performed in the following sections, the FFR control structure, depicted in Figure 3, is implemented as in [40].

Only wind turbines and wind power plants are considered for the FFR implementation. The reason is that PV plants require active power reserve or energy storage equipment in order to provide FFR. Additionally, the FCR from ReGen plants is not included in the scope of this document.

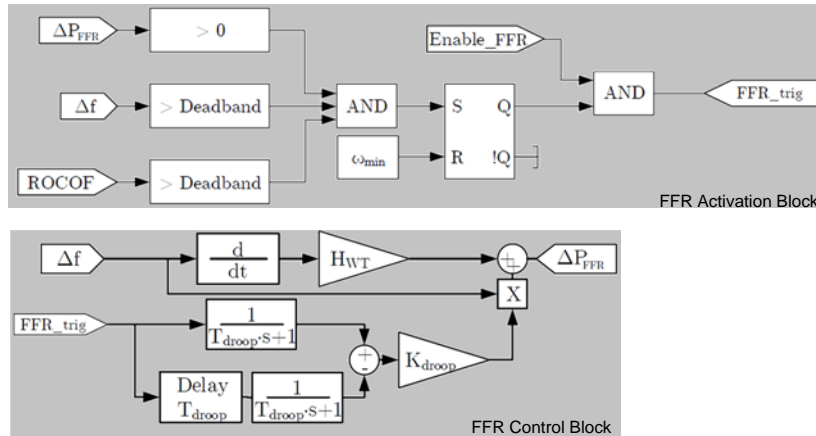


Figure 3: FFR control structure overview.

## 4.1 Motivation

Several studies in the literature [7-10] have shown that wind power plants (WPPs) can provide FFR to enhance the stability of power systems with large share of wind power. Nevertheless, the results illustrate that the power system stability can be made worse without a careful coordination between WPPs providing frequency support. There is a crucial need for frequency support coordination between WPPs in power systems with large displacement of conventional power plants by wind power.

Two set of studies, showing the need for coordination between WPPs in FFR provision both in island power systems as well as in large interconnected power system, are presented in the following showing this aspect.

### 4.1.1 Need for frequency support coordination from WPPs in island power system

This study, described in details in [11], is conducted with an aggregated wind power plant model integrated into a generic island power system model [9], specifically designed to assess FFR in a relatively simple but still relevant environment. This generic test system, depicted in Figure 4, is small enough to be able to keep a good track of the system characteristics, and at the same time appropriate to display phenomena of interest for power system stability.

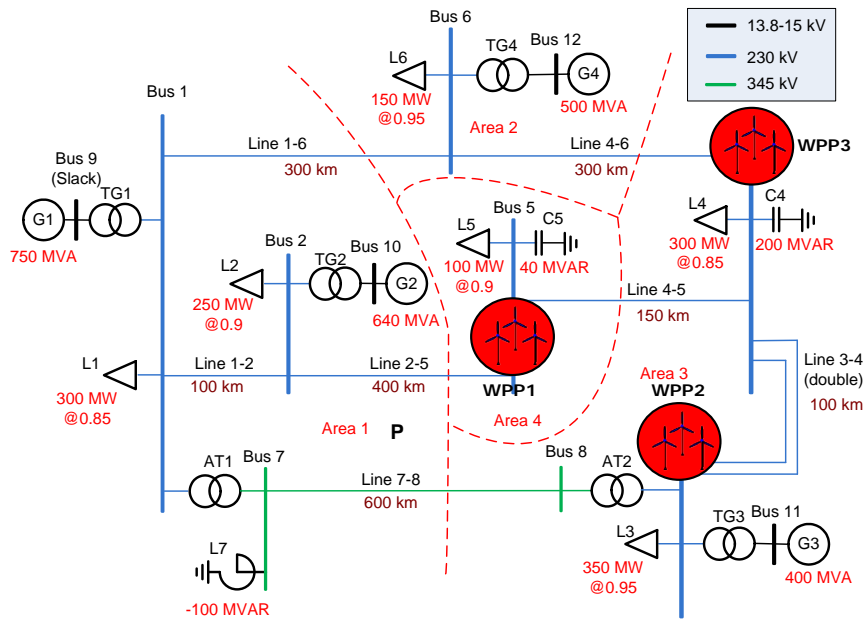


Figure 4: Generic island power system with multiple WPPs [10].

A set of simulations, considering different wind power penetrations levels and WPPs' locations, are carried out in [10-11] to reflect how power system stability may be affected when WPPs are required to simultaneously contribute with FFR. A 50% wind power penetration<sup>1</sup> scenario is conducted by decommissioning large conventional units and connecting additional WPPs into the system, namely three WPPs in three different locations, as depicted in Figure 4.

Figure 5 depicts the frequency excursion following the loss of largest generation for 50% scenario in different cases, i.e. firstly without any FFR provision, then with FFR enabled in one, two or three WPPs, respectively. The basic case in Figure 5 corresponds to 0% wind power penetration, namely where no WPPs are connected into the system. Notice that the displacement of conventional units by accommodation of 50% wind power without any FFR provision, decreases the system inertia and the frequency nadir, easily exceeding the load shedding limits (i.e. 0.98pu). Notice also that WPPs with FFR provision improve both system inertia and frequency nadir, as well as that the frequency nadir, when all WPPs simultaneously provide FFR, is improved compared to the base case.

The displacement of conventional power plants by WPPs, reflected in this work through the 50% scenario, may increase drastically the complexity of the power system operational characteristics.

As depicted in Figure 5, the power system performance might be degraded if, without detailed insight and understanding of this complexity, all WPPs in the system simultaneously provide FFR. For example,

<sup>1</sup> The wind power penetration is understood as the amount of the load demand which is provided by online wind power capacity.

Figure 5 shows how a double frequency dip may occur in the frequency excursion when more than one WPP simultaneously provides FFR. This double frequency dip, typically not preferred by power system operators with few exceptions [3], [12] shows that it might not be necessary that all WPPs simultaneously provide FFR – as for example shown in

Figure 5 the frequency excursion in the scenario with FFR only enabled in WPP1 and WPP2 is almost the same, except the double dip in the frequency, with that with FFR enabled in all three WPPs.

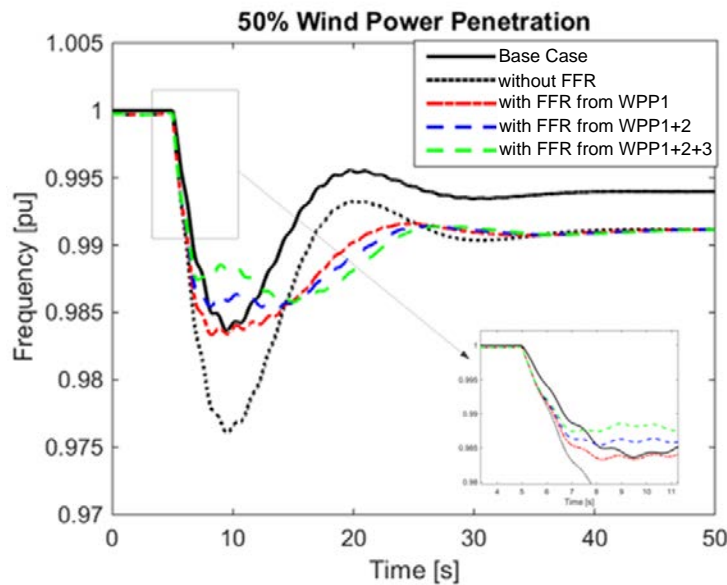


Figure 5: System frequency excursion following the loss of largest generator for a 50% wind power penetration with and without FFR from WPPs.

The results show that it is not enough only to require WPPs to exhibit technical capabilities to provide enhanced services, but it is also crucial to coordinate the FFR’s provision between WPPs in order to ensure a future resilient power system. A careful coordination of the FFR provision between WPPs, considering for example different activation times and parameter tuning, might be necessary for each particular network.

#### 4.1.2 Need for frequency support coordination from WPPs in large scale power system

Similar to the island study case above, a generic large scale power system model is simulated in order to analyze the need for a coordinated frequency support from WPPs and also investigate the impact of the FFR parameters on the frequency control dynamics of the power system. The frequency control dynamics of a generic large scale power system is represented as a single-bus model including various governor and turbine models such as steam, hydropower, and nuclear power plants. This model is illustrated Figure 6. It is adapted from [20] in order to simulate 4<sup>th</sup> November 2006 incident in ENTSO-E for iTesla project [21].

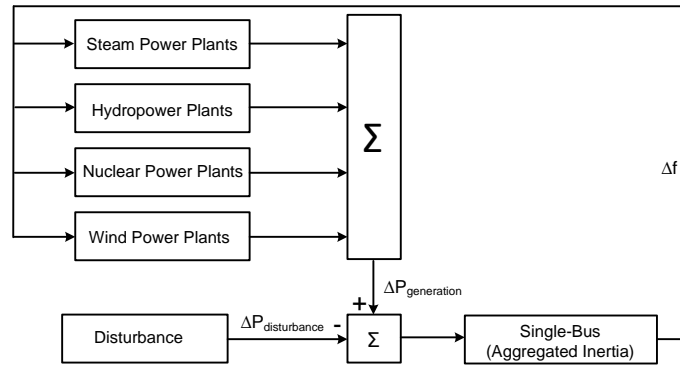


Figure 6. Single-bus model of a generic large scale power system with WPPs

Different wind power penetration levels are implemented in this model in order to reduce down the inertia by replacing steam and nuclear power plants. Each penetration levels of wind power are assumed as a scenario in this study. These scenarios are summarized in Table 4. The penetration level is the defined as the ratio of wind power generation to total power generation.

Table 4. Different Wind Power Penetration Scenarios

Penetration [%]	Total Generation [GW]	Steam [GW]	Hydro [GW]	Nuclear [GW]	Wind [GW]
10	68	45	6	10	7
20	68	38	6	10	14
30	68	33	6	8	21
50	68	25	6	3	34

A set of simulations, considering the penetration levels in Table 4 are carried out to analyze the impact of these penetration levels of frequency stability of the generic power system when WPPs are required to contribute with the FFR. All WPPs are modeled as aggregated in these simulations and the simulation results are given in Figure 7 for 30% and 50% wind penetration scenarios. Until 30% wind penetration, the power system frequency dynamics are improved in terms of the frequency nadir (i.e. minimum frequency point) and the time to reach quasi-steady state frequency. Due to the further decrease in the power system inertia and the wind speed variations, in 30% and 50% wind power penetration scenarios, a secondary frequency dip is occurred which is not acceptable by TSOs.

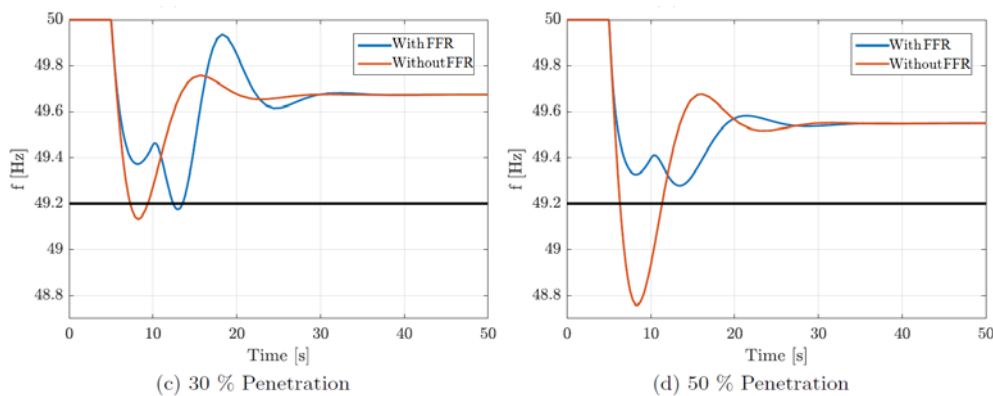


Figure 7. System frequency excursion following the loss of a generator for the 30% (a) and 50% (b) wind power penetration with and without FFR from WPPs

Similar to the islanded power system simulations, the results in Figure 7 show that it is not enough only to require WPPs to exhibit technical capabilities to provide FFR with one set of parameters, but it is also crucial to coordinate the FFR between WPPs depending on their active power production (i.e. average wind speed) and their installed capacities (i.e. wind power penetration level). In order to improve the power system frequency dynamics without a secondary frequency dip, a coordination of the FFR provision from different WPPs, can be required for high penetration levels considering parameter tuning with different activation times and controller gain values. However, such coordination might be a regulatory challenge in practice when different WPP owners might be involved.

In this study, two approaches are developed in order to tune the FFR of WPPs in the generic power system (Figure 6) with the 50% wind power penetration level (Table 4). In the first approach, the aggregated FFR of WPPs is optimized by tuning the parameters with a meta-heuristic optimization algorithm. Aggregated WPP model is simulated in this approach according to the assumption that all WPPs have the same average wind speed. Therefore, in order to represent the geographical distribution of WPPs, the second approach is developed with three WPPs which have different wind speeds. The parameters of the FFR in these WPPs are tuned with the meta-heuristic optimization algorithm by using the investigation results of the first approach. In the following sections, the details of these approaches are presented with the simulation results.

An optimization approach is designed for parameter tuning of the FFR in WPPs. The optimization approach consists of the power system model, which has conventional power plants, the wind power plants with the FFR implementation and the optimization engine. The illustration of the optimization approach is given in Figure 8. As mentioned earlier, this framework is used for the aggregated and distributed FFR of WPPs. This developed approach is implemented in the TSO level. Since TSOs have full control and information on their area, the optimization approach can be simulated offline in TSO level (i.e. in the planning stage of the FFR).

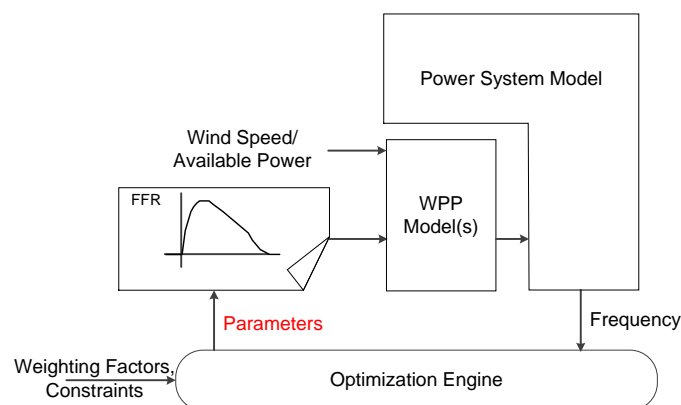


Figure 8. Illustration of the Optimization Approach of FFR from WPPs

In Figure 9, the control structure is illustrated including TSO level, aggregator level, and plant level. In the planning stage at the TSO level, the optimization engine (Figure 8) is running and generating the optimum parameters depending on the different wind speeds/available power. These optimum parameters are sent to the aggregator level which can be owned by the WPP owners. In the aggregator level, depending on the available power values of WPPs, the parameters are dispatched to each WPP. After the dispatch through

communication infrastructure, the parameters are sent to each WPP. According to the control structure, the FFR is implemented in plant level, the dispatch is in aggregator level, and the optimization engine is in TSO level. The communication channels are mainly used between the aggregator and plant levels.

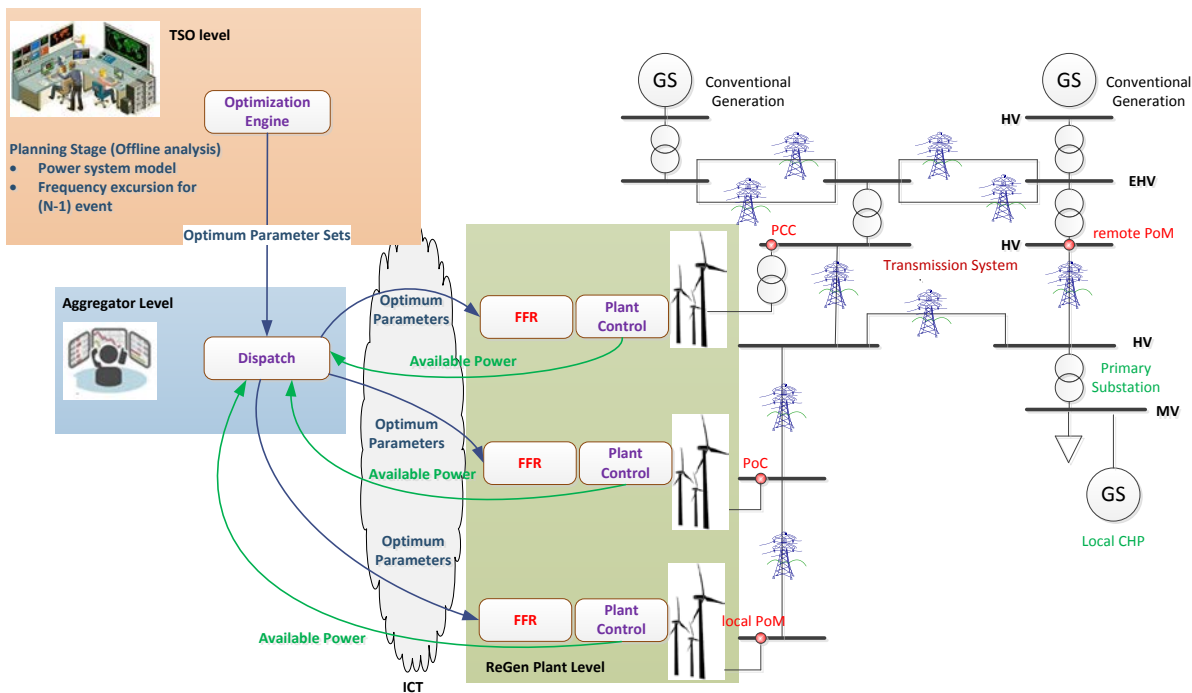


Figure 9. Implementation of Offline Optimization Approach with Control Levels

## 4.2 Optimization of Aggregated FFR from WPPs

In this optimization approach, the aggregated WPP model [40] is employed with a FFR controller. The implementation of the FFR controller will be later explained in this section. Using the implementation in Figure 8, the genetic algorithm (GA) is selected to optimize the parameters of the aggregated FFR of the WPPs. The reason of selection the GA is the non-linearity of the problem with the non-linear constraints in WTs and the wide-spread use in power system studies.

The GA imitates the selection process of biological evolution [22]. In the first iteration, the algorithm creates a random population while taking constraints and limits into account. Based on the performance of each member of the population, their so-called fitness value, a new population set is created. The new population, or children, is created by either crossover, mutation or simply passing on the genes of the parent population. In this way, the optimization process is based on the suitability of parameters instead of randomly varying parameters until all combinations are calculated. For instance, passing on the parents' genes with the best fitness values to the next generation secures that these genes survive, while the crossover children are equipped with the best vector entries from both parents to form a possibly improved vector. Additionally, randomly determined mutations result in more diverse children and thus a more diverse population. Employing this approach improves the fitness of each generation until the terminating condition is reached, e.g. the relative change in fitness value is lower than a specified tolerance value.

The GA requires an objective function to minimize the fitness value of this function. In the present study, the objective is to improve the frequency response dynamics of the power system model by minimizing the frequency nadir, secondary frequency dip (if there is), and the time to reach the quasi-steady state during the FCR (i.e. 30 sec. [5]). Therefore with these three operational metrics, the objective function is defined in Equation (1) for the multi-objective optimization problem. In Equation (1),  $\Delta f_{nadir}$  is the frequency deviation at the frequency nadir,  $\Delta f_{2^{nd} dip}$  is the frequency deviation at the secondary frequency dip, and finally  $t_{SS}$  is the time to reach the quasi-steady state of the FCR. At the each iteration of the GA, the power system model is simulated with the selected parameters of the FFR in MATLAB/Simulink. The results of the simulation are evaluated and the GA tries to minimize the objective function.

$$ObjFunc = \alpha_1 \Delta f_{nadir} + \alpha_2 \Delta f_{2^{nd} dip} + \alpha_3 t_{SS} \quad (1)$$

The weighting factors  $\alpha_1$ - $\alpha_3$  can be selected according to the power system frequency dynamics and the TSO's decision. In this work, the frequency nadir improvement has the highest priority. The other operational metrics, the secondary frequency dip and the time to reach the quasi-steady state, are not the focus since there are no clear regulations from power system operators. Therefore, the weighting factors are selected 0.5, 0.35, and 0.15 respectively. These values are obtained by performing a sensitivity analysis in the power system model.

After the evaluation of the objective function (in Equation (1)), the GA selects the best parameters of the FFR for the new iteration. Accordingly, it continues to minimize the value of the objective function until the relative change is less than the function tolerance. The implementation of the GA is given in Figure 10.

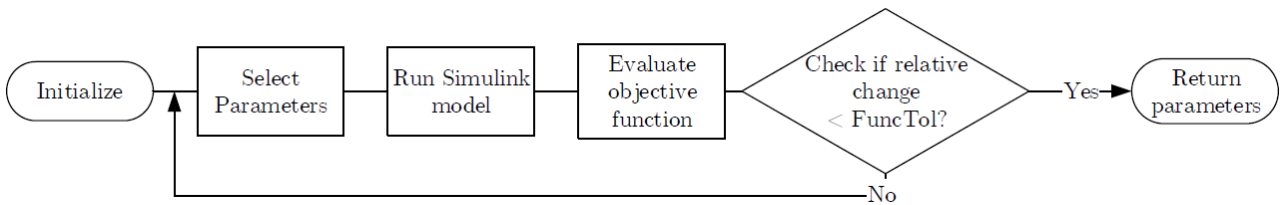


Figure 10. Block diagram of the GA implementation for the FFR parameters

This implementation is employed for two types of FFR control structure in order to optimize the aggregated FFR. Two controllers are illustrated in Figure 11. These two controllers are representing the state-of-the-art FFR. The first control structure in Figure 11a can be assumed as an open-loop response, and it is employed to investigate the active power profile during the frequency excursion in terms of ramp-up, ramp-down rates, magnitude and duration of the profile. The second control structure Figure 11b is more a closed loop control, which detects the frequency deviation and rate of change of frequency (ROCOF) and responds depending on these two signals.

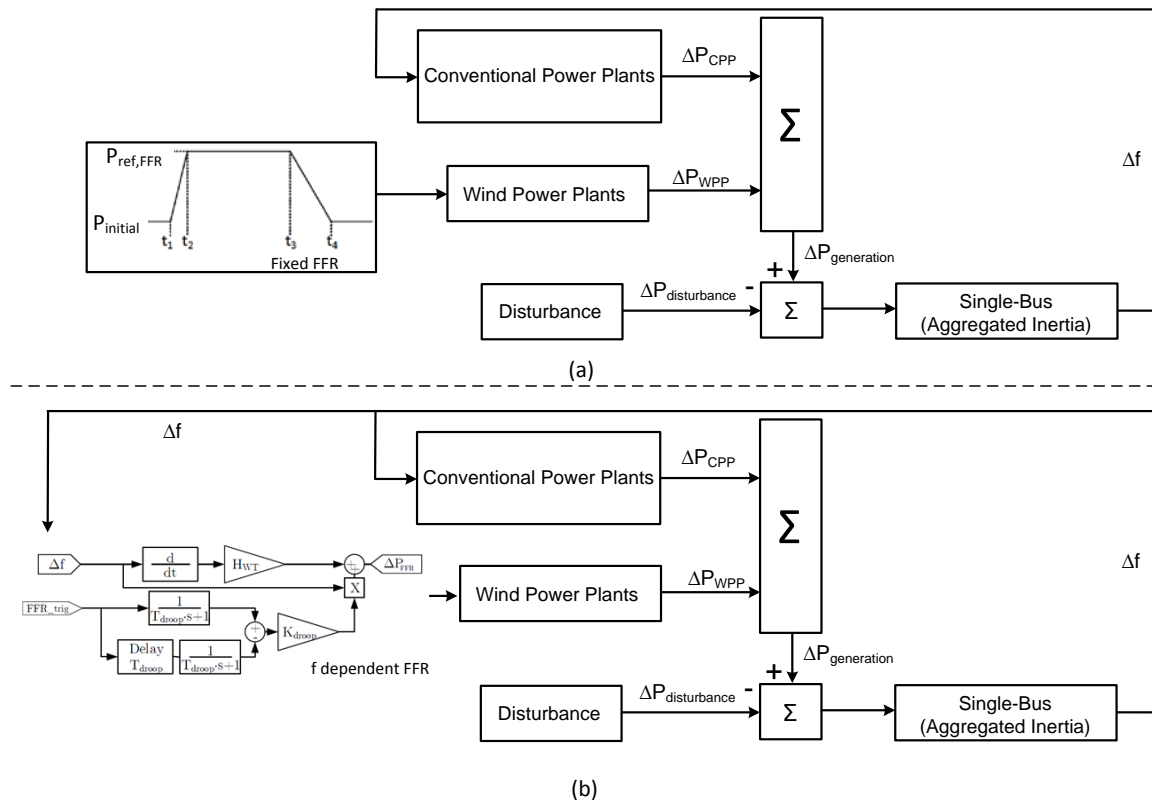
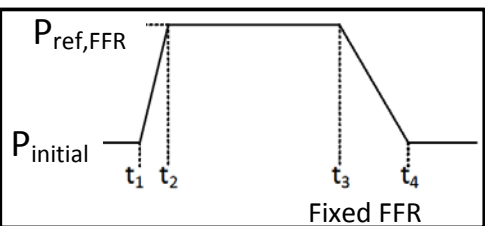
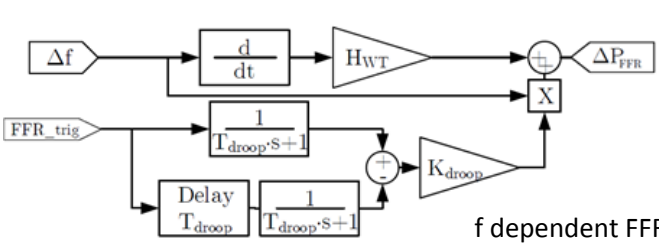


Figure 11. FFR control structures; (a) Fixed FFR control, (b) Frequency dependent FFR control

The parameters of the two controllers, which are defined as decision variables in the GA, are optimized offline to find the optimum aggregated FFR for the 50% wind penetration scenario. These parameters are listed in Table 5. The modelling details of the conventional power plants, WPPs, and penetration scenarios can be found in [41]. Beside these scenarios, various wind speeds are selected regarding the operation regions of the WT

Table 5. FFR parameters as decision variables for the optimization algorithm

Fixed FFR Control		Frequency dependent FFR Control	
			
$P_{ref,FFR}$	fixed active power reference during FFR	$T_{droop}$	temporary droop time constant
$t_1$	start time of the FFR	$K_{droop}$	temporary droop gain
$t_2$	time decides the ramp-up rate	$H_{WT}$	derivative gain
$t_3$	time decides the ramp-down rate	$T_{FFR}$	duration of FFR
$t_4$	end time of the FFR		

The optimized simulation results of the first controller are given in Figure 12. According to these results, when all WPPs are operating at the 11 m/s, there is no support for the frequency nadir. As expected, at above rated wind speed (14 m/s) has better performance since there is no recovery period after the FFR. Further constraint in the optimization algorithm can be included as a limitation for the  $t_4$  parameter, if the long duration of the overloading of WPPs is not allowed. Finally, for wind speeds (7 m/s), the aggregated FFR is feasible regarding the frequency response of the overall system (Figure 12a) and the impact of the recovery period (Figure 12b).

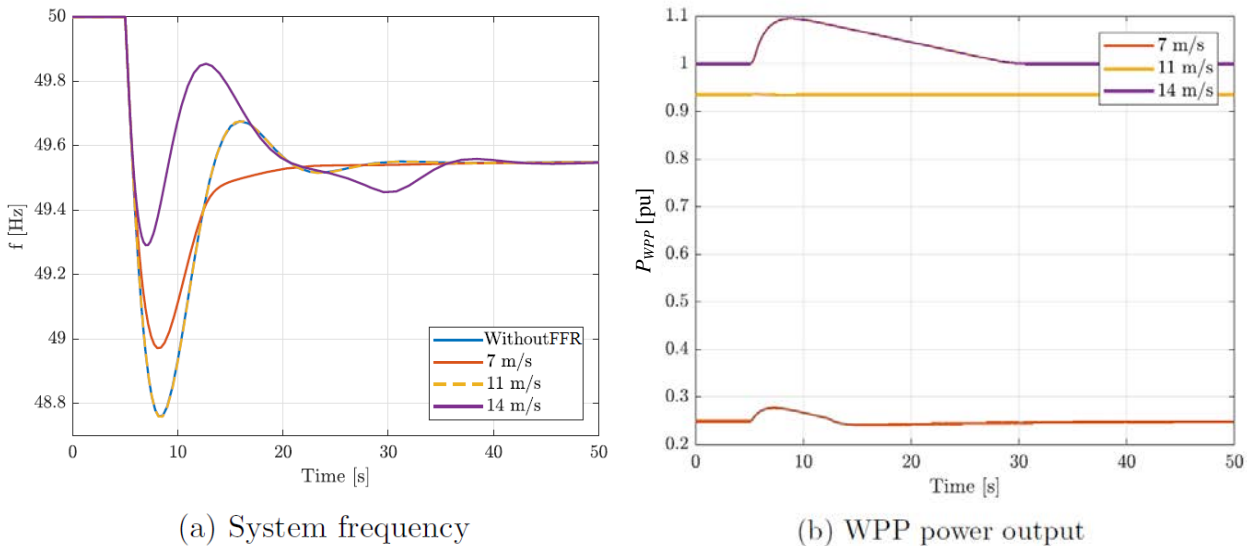


Figure 12. Optimization results of fixed FFR control for 50% wind power penetration

The optimization results of the frequency dependent FFR are given in Figure 13. Compared to the previous case, the results are more realistic since the FFR is dependent on the frequency dynamics. The difference between the performances of the fixed FFR and the frequency dependent FFR can be clearly seen at the operating point close to the rated wind speed (11 m/s). However, when the FFR is activated at 11 m/s, the secondary frequency dip is observed due to the recovery period. Another improved result is obtained at the high wind speed (14 m/s). With the frequency dependent FFR control, the released energy released during the response is reduced with a better frequency nadir compared to the fixed FFR control. This result is reasonable due to the close loop structure of the  $f$  dependent response and the volume of the response is not pre-defined for a constant value.

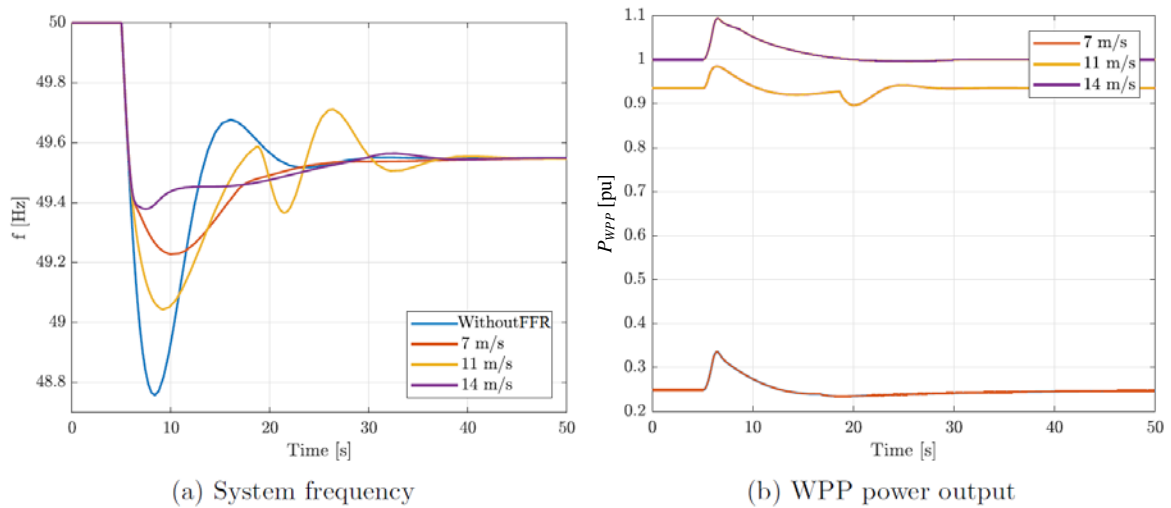


Figure 13. Optimization results of frequency dependent FFR control for 50% wind power penetration

The comparison of the operational metrics, which are the relative change in the frequency nadir and the time to reach the minimum frequency point according to no FFR control, is shown for the fixed and the frequency dependent FFR control in Figure 14.

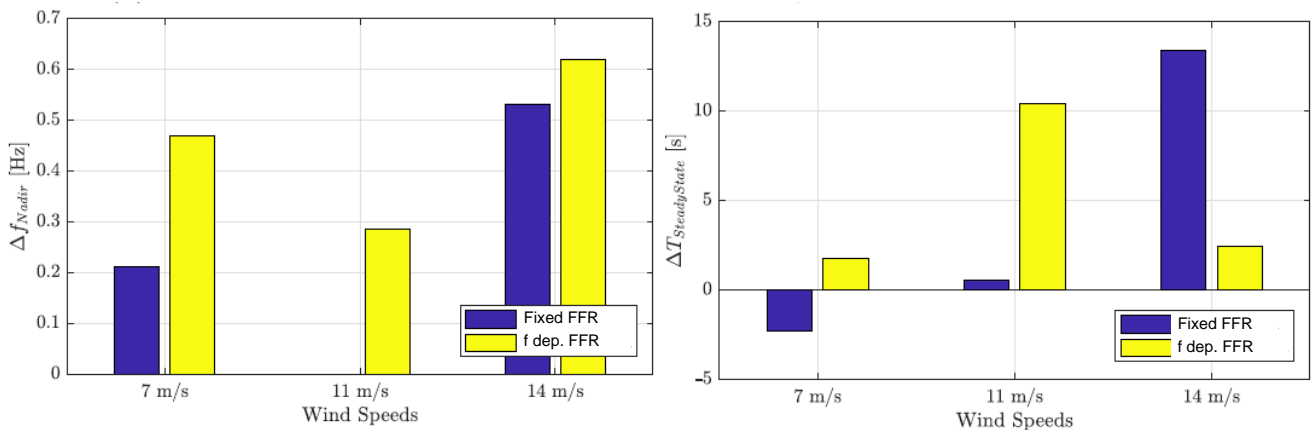


Figure 14. Relative change in frequency nadir and time to reach the steady-state for 50% wind power penetration

When the aggregated WPP is considered with a single wind speed input, the optimization results can be employed to estimate the average response of the WPPs for different wind power penetrations. However, the above presented results are not sufficient to investigate the FFR of many geographically distributed WPPs which are operated by different owners. **Additionally, the control implementation cannot be realized with the aggregated WPP assumption.** Therefore in the following section, in order to represent the different wind speeds, the coordinated FFR of WPPs is investigated considering three WPPs, which are equipped with the frequency dependent FFR control.

### 4.3 Optimization of Coordinated FFR from WPPs

In order to expand the previously presented approach (aggregated FFR), a new approach is developed with the implementation of three individual WPP models into the power system model (Figure 6). In this approach, the coordinated control of WPPs is investigated by optimizing the WPPs' FFR parameters. Accordingly, the coordinated control approach employs the GA to analyze the allocation of the FFR from different WPPs in terms of the activation time, the duration, and the magnitude. It can be assumed as an offline coordination of WPPs as a system wide analysis where the generation schedule of conventional power plants and the wind power penetration level is known. Furthermore, the results presented later in this section can be used to implement novel control strategies for individual WPPs or WPP clusters.

The developed approach employs the GA to coordinate the FFR of three WPPs with respect to a reference shape of their active power contributions. This reference power shape is obtained from the aforementioned approach where the aggregated FFR is optimized for above rated wind speeds (i.e. 14 m/s). If the overall active power output of WPPs is as close as possible to the reference shape, the optimum parameters can be achieved with sufficient support to the FCR. The simulation setup for the coordinated FFR is illustrated in Figure 15 with the reference power shape. It has to be noted that this shape is obtained from an aggregated WPP model without a rate limiter in the FFR control to represent an ideal case. It is therefore not expected that the GA will be able to directly replicate the reference shape.

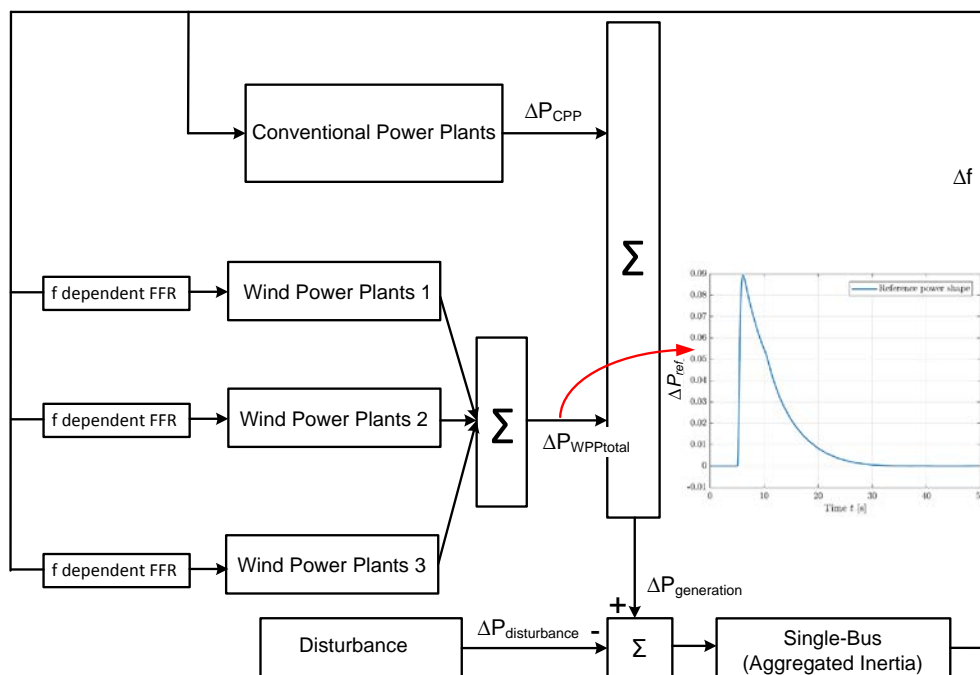


Figure 15. Simulation setup with reference power shape for the optimization algorithm

The idea behind the coordinated FFR is to have the reference power shape without the recovery period which corresponds to the operation at above rated wind speed conditions. In order to implement this idea in the GA, the objective function is proposed in Equation (2).  $P_{ref,i}$  is the reference shape,  $P_{WPPtotal,i}$  is the actual simulated active power during the optimization.  $i$  represents the simulation time steps,  $t_{nadir}$  is time to reach the frequency nadir. Finally,  $t_{end}$  is the total time of the simulation.

$$ObjFunc = \sum_{i=t_{start}}^{2t_{nadir}} \alpha_1 |P_{ref,i} - P_{sim,i}| + \sum_{i=2t_{nadir}}^{t_{end}} \alpha_2 |P_{ref,i} - P_{sim,i}| \quad (2)$$

The weighting factors ( $\alpha_1$  and  $\alpha_2$ ) divided the total response into two parts. The first part around the frequency nadir comprises the summation of the error values between simulated and reference powers ( $|P_{ref,i} - P_{sim,i}|$ ) from the event time to twice of the time to reach the nadir. The second part is the summation of the remaining errors until the end of the simulation, as given in Figure 16. For the optimization study, in the second part  $\alpha_2$  is assumed as 1, while in the first part  $\alpha_1$  is increased due to the high priority of improving the frequency nadir. Therefore, small errors in the first part will improve the fitness value of the GA more than the second part. These weighting factors can be selected depending on the WPPs' operating conditions or the TSO's operating decision. For instance, if the power system is the fast governor dominated (e.g. gas power plants), the second weighting factor can be small to decrease further the frequency nadir. Or in a hydro power plant dominated power system, the second coefficient can be more important depending on the FCR performance of the hydro power plants.

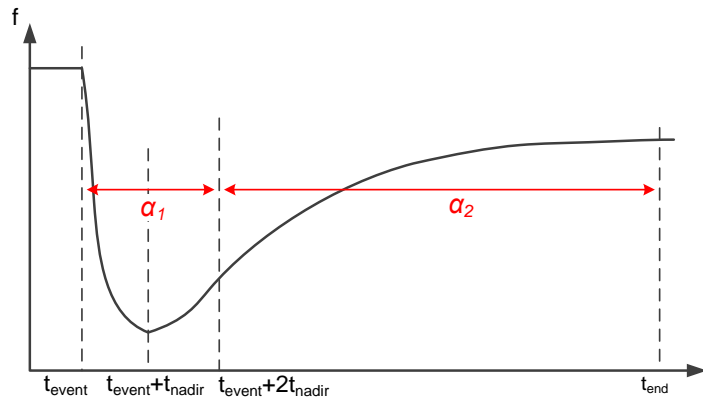


Figure 16. Weighting factors of objective function depending on frequency shape

After conducting simulations for various wind speeds, it is observed that the defined objective function (Equation (2)) is not sufficient enough to improve the secondary frequency dip due to the recovery period of WTs. In order to improve the objective function, a penalty value is introduced. The assessment of the penalty value is based on the trumpet characteristic which is inspired from the quality assessment of the primary and secondary frequency control [19]. The trumpet characteristic is implemented based on the frequency nadir and the quasi-steady state. Accordingly, the characteristic represents an under-frequency constraint for each simulation in the optimization. If the system frequency undergoes this constraint during the simulation, the penalty value is added to the objective function at the end of the iteration. Therefore, the GA can eliminate this solution due to the secondary frequency dip.

The trumpet characteristic  $H(t)$  is illustrated in Figure 17. Additionally, it is formulated in Equation (3).  $f_{quasi-ss}$  is the quasi-steady state frequency value,  $f_{nadir}$  is the minimum frequency value, and  $f_{nom}$  is the nominal frequency.  $t_{nadir}$  is the time to reach the frequency nadir. Additionally,  $d$  is defined the difference between the  $f_{nadir}$  and the initial value of the trumpet characteristic. This is tunable and in this optimization study, it is 20 mHz and assumed as a design band [5].

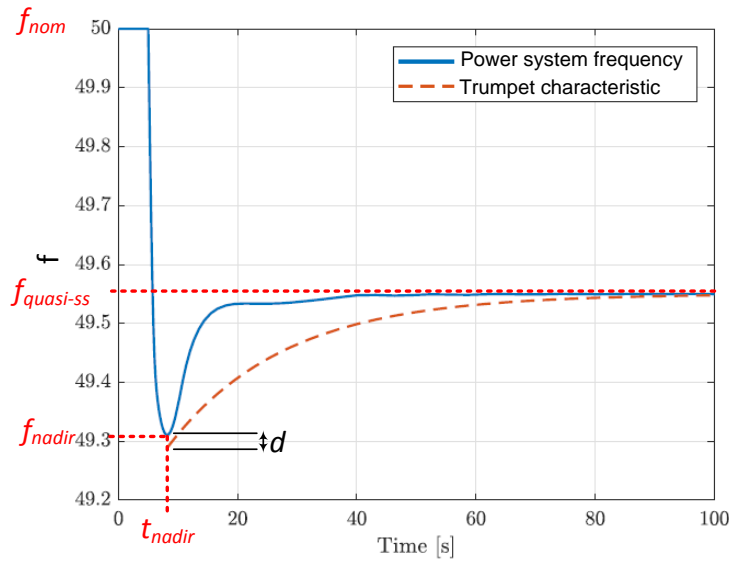


Figure 17. Trumpet characteristic for penalty assessment of the objective function

$$\begin{aligned}
 H(t) &= f_{quasi-ss} - Ae^{-\frac{t-t_{nadir}}{T}} \\
 A &= f_{quasi-ss} - f_{nadir} + d \\
 T &= \frac{f_{nom}}{\ln(A/d)}
 \end{aligned} \tag{3}$$

After the implementation of the GA with the power system model (Figure 15) and the objective function (Equation (2) and Equation (3)), the simulations are performed. Different wind speeds are assumed for three WPPs and these cases are summarized in Table 6. These cases are conservative since the wind speeds close to the rated wind speed is focused more than the other wind speeds. Accordingly, for the first and second part, only  $(N-1)_{max}$  contingency event where, 5100 MW trips, is considered and the optimization is performed for this severe event. In the third part, the result of the optimization for Low&Med case (7,11, and 11 m/s) is simulated for less severe events compared to  $(N-1)$ .

Table 6. Cases for optimization of the coordinated FFR from WPPs

Cases	WPPs' Wind Speeds				
			WPP1	WPP2	WPP3
<b>Uniform Wind Speed Cases (Part 1)</b>	1	Low	7	7	7
	2	Medium	11	11	11
	3	High	14	14	14
<b>Non-uniform Wind Speed Cases (Part 2)</b>	4	Distributed	7	11	14
	5	Low&Med	7	11	11
	6	High&Med	14	11	11
<b>Cases for Less Severe Events (<math>&lt; (N-1)_{max}</math>) (Part 3)</b>	7	75% of $(N-1)_{max}$	7	11	11
	8	50% of $(N-1)_{max}$	7	11	11
	9	25% of $(N-1)_{max}$	7	11	11

The simulation results of the optimal FFR from three WPPs are presented for uniform wind speed cases in Figure 18. All the WPPs have the same wind speeds in each case as 7, 11, and 14 m/s respectively. Additionally, the previously obtained parameters in the aggregated FFR optimization are employed in each WPP. The simulations are performed and compared in terms of power system frequency (Blue line in the power system frequency results) with the coordinated FFR.

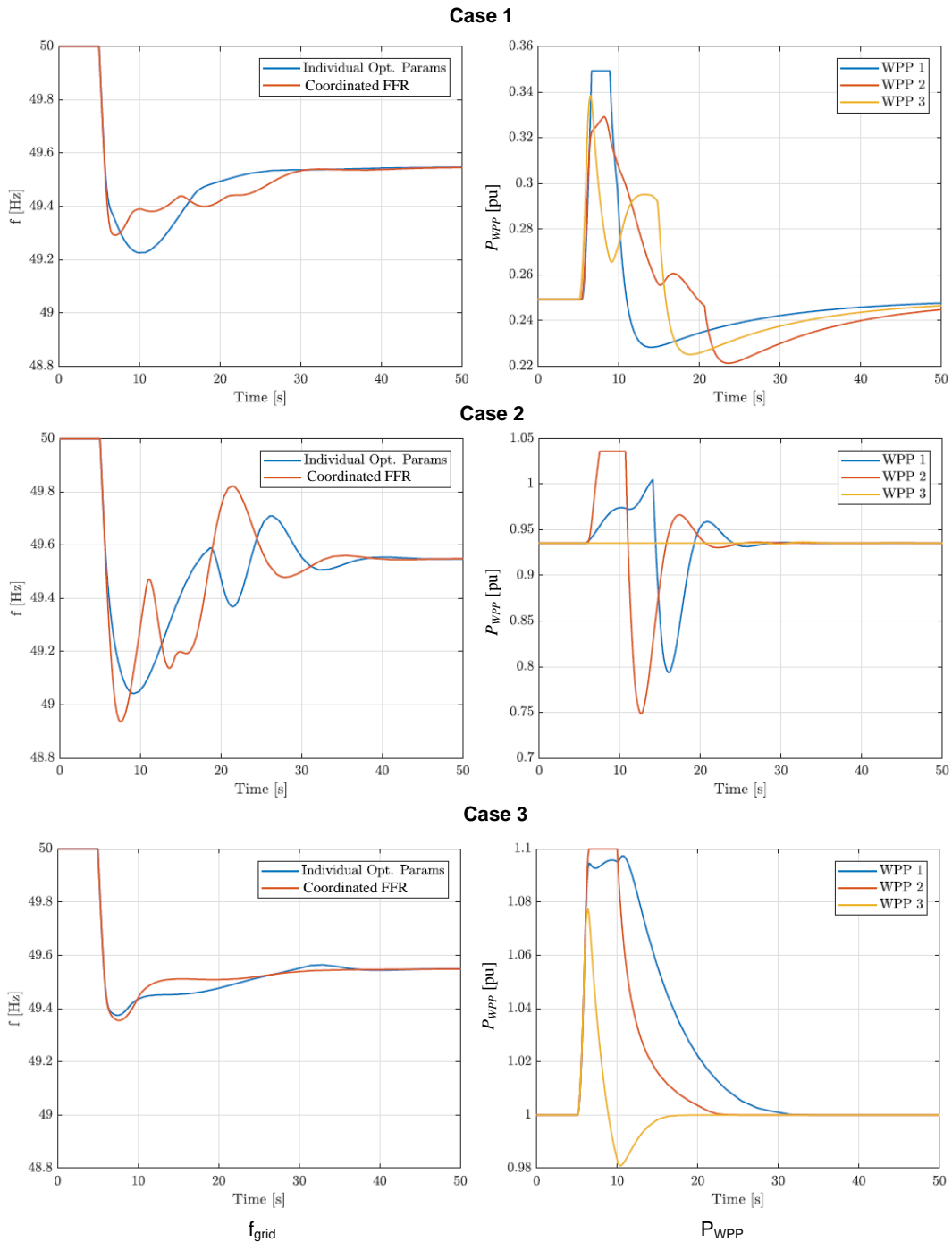


Figure 18. Power system frequency ( $f_{grid}$ ) and WPPs' active power outputs ( $P_{WPP}$ ) at uniform wind speed conditions

In Case1, by coordinating the FFR duration, each recovery period is distributed among WPPs to reduce their impacts on the secondary frequency dip. Namely, return to normal operation of each WPP is consecutively delayed by 5 seconds due to the optimization. WPP1 (blue line) terminates its frequency support after 10 seconds. WPP 2 (red line) and 3 (yellow line) continue their support for other 10 and 5 seconds, respectively. Furthermore, the kinetic energy released from the WPPs is more balanced instead of demanding more by one or two WPPs.

In Case 2, the prevailing wind speeds at each WPP are increased to 11 m/s, and the power system operation is critical in terms of the large active power drops at the recovery period. Any delay in providing active power through the FFR will accordingly postpone the secondary frequency dip and the corresponding oscillations in the power system frequency. However, in this case the coordinated response doesn't perform better than the individually tuned parameters for the aggregated FFR. This is due to the objective function and the selection of the weighting factors.

In the last case (Case 3) with the uniform above rated wind speeds, the FFR has already the advantage due to excess available power (or no recovery period). Therefore, coordinating the inertial support is not expected to cause a large improvement. Considering the comparison between the individually tuned response (blue line) and the coordinated response (Red line) in Figure 16 (Case 3), it is observed that the difference in frequency nadir is around 20 mHz. However, by coordinating the duration of the inertial response, it is possible to reduce the time to reach quasi-steady state by around  $t = 10$  s. This has the advantage of slightly improving the performance of the overall FCR.

After optimizing the same wind distribution of different WPPs, more realistic optimization study is conducted by assuming different wind speeds for each geographically distributed WPP. In Table 6 (second part), the non-uniform wind speed cases focused comprising more 11 m/s wind speed that has more challenging due to the recovery period and the secondary frequency dip. The optimized simulation results are given in Figure 19. As it is compared in the Case 1, Case 2, and Case 3, the coordinated FFR is compared with the individually optimized parameters in terms of the performance of the power system frequency.

In Case 4, with the coordinated approach, the time to reach the quasi-steady state is reduced around 15 s. However, when the WPPs' outputs are considered, WPP3 which has 14 m/s wind speed provides the FFR for 25 s (Figure 19). Another important remark is that the WPP with medium wind speed doesn't have any impact on the FFR. This is an important outcome of the optimization of the coordinated FFR if the secondary dip wants to be avoided.

In Case 5 with WPPs' operating wind speeds at 7, 11, and 11 m/s, the secondary frequency dip and following oscillations in the power system frequency response are expected. By coordinating the respective FFR from WPPs, the power system frequency is improved regarding the oscillations and the time to reach to the quasi-steady state. The main contributors are WPP1 and WPP3 while WPP2 has a less contribution. However, the FFR parameters of WPP2 are optimized such that it reacts to the secondary dip caused by WPP3.

Case 6 includes both medium and high wind speeds (Table 6). Compared to the result of the individually optimized parameters, the coordinated FFR can slightly improve the frequency nadir by 50 mHz as shown in Figure 19 (Case 6). Furthermore, the time to reach the steady state is reduced together with the oscillations

in the power system frequency. The secondary dip oscillations still cannot be avoided due to the high amount of wind power operating close to rated wind speed. However, the coordination of WPPs helps to reduce the dip severity by injecting additional active power at the right moment.

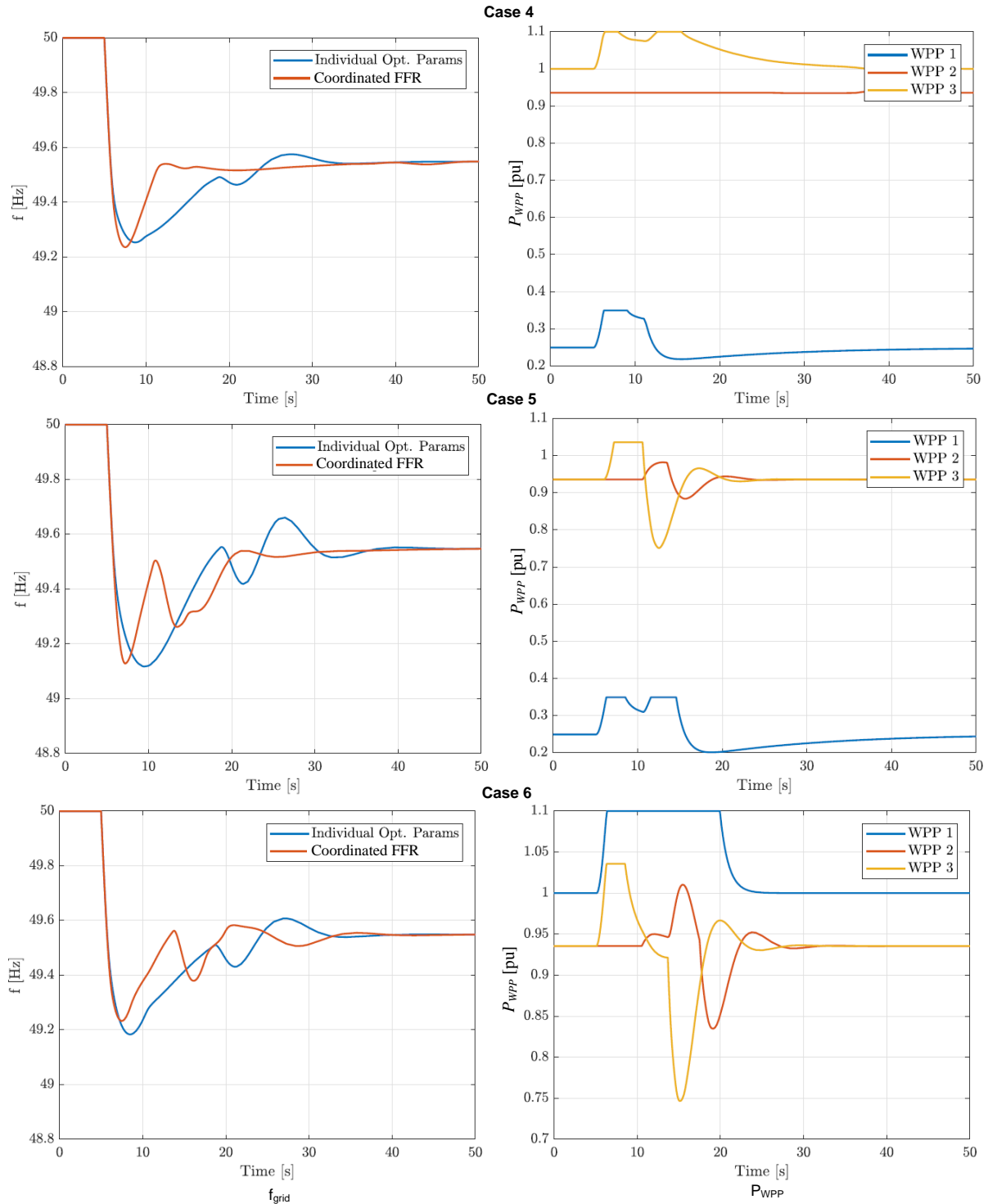


Figure 19. Power system frequency ( $f_{grid}$ ) and WPPs' active power outputs ( $P_{WPP}$ ) at non-uniform wind speed conditions

Finally, case 7-9 are simulated for WPPs with 7, 11, 11 m/s average wind speeds to investigate the impact of the optimal parameters during less severe events compared to the maximum contingency which is 5100 MW trip of the generation. In Figure 20, the results are given and it can be seen that even without fine tuning, WPPs can support the frequency stability without any deterioration. However, for these cases, the secondary dip is increasing which does not have the priority when the weightings are selected. Therefore, the results are expected and further improvements can be considered by running more cases depending on the operators' needs.

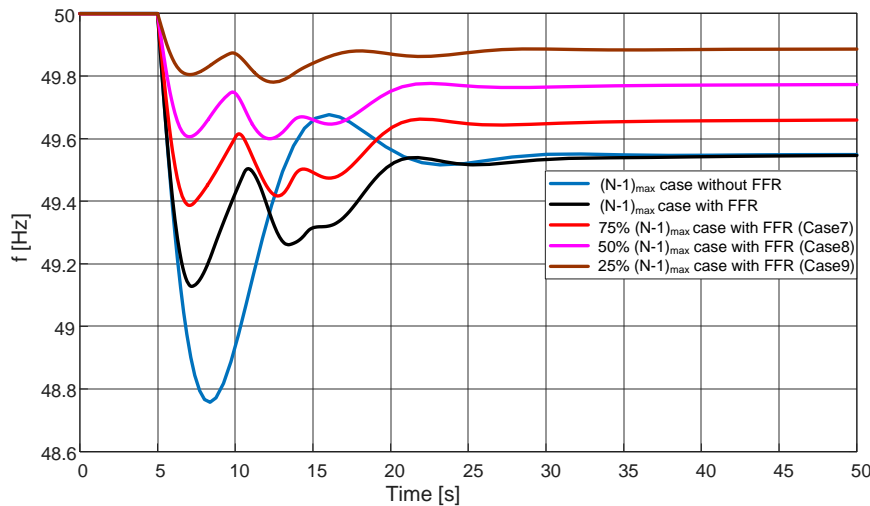


Figure 20. Power system frequency ( $f_{grid}$ ) for test cases 7, 8 and 9 where WPPs operate at 7, 11, and 11 m/s average wind speeds

#### 4.4 Analysis of WT's FFR Performance

After analyzing the aggregated and coordinated FFR from WPPs, in this section, the FFR performance of the single WT is analyzed and is quantified by maximizing the released energy considering the WT's mechanical and electrical limitations. Similar to the previous sections, the GA is employed for the optimization algorithm for releasing the maximum energy during the FFR. Accordingly, the FFR in this section is formulated as the fixed FFR control as in Section 4.2. The GA optimizes the duration of the overproduction period ( $\Delta T_{over}$ ) for different pre-defined active power references of the WT ( $P_{ref,FFR}$ ). The illustration of the optimization algorithm is given in Figure 21. Finally, the contribution of the optimization study is further extended by analyzing the impact of the FFR on the loading of the WT structural components.

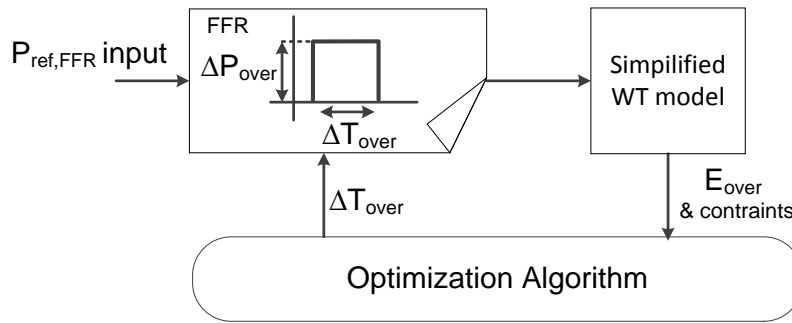


Figure 21. Illustration of Optimization of Wind Turbine's FFR

Aforementioned approach maximizes the total released energy during FFR by optimizing  $\Delta T_{over}$  while  $\Delta P_{over}$  (Figure 21) is kept constant during the optimization at a predefined value between 0.01 to 0.3 pu. The optimization results (i.e. overproduction period versus power overproduction set points) are given in Figure 22 (a) for different wind speeds. According to these results, it is clear that the maximum energy which can be extracted out of the WT within the defined electrical and mechanical constraints is achieved for the wind speed of 7m/s. It is also worth noticing that the pattern of the optimized results is similar between wind speeds 6 m/s to 9 m/s in terms of the maximized energy. However, close to the rated wind speed the drop in the optimum power is very steep due to the MPPT control. This conclusion is quite interesting as one would expect to extract more energy at higher wind speeds even within the defined constraints. Accordingly, any control attempt demanding a large energy during very short overproduction duration should be designed carefully due to the recovery period.

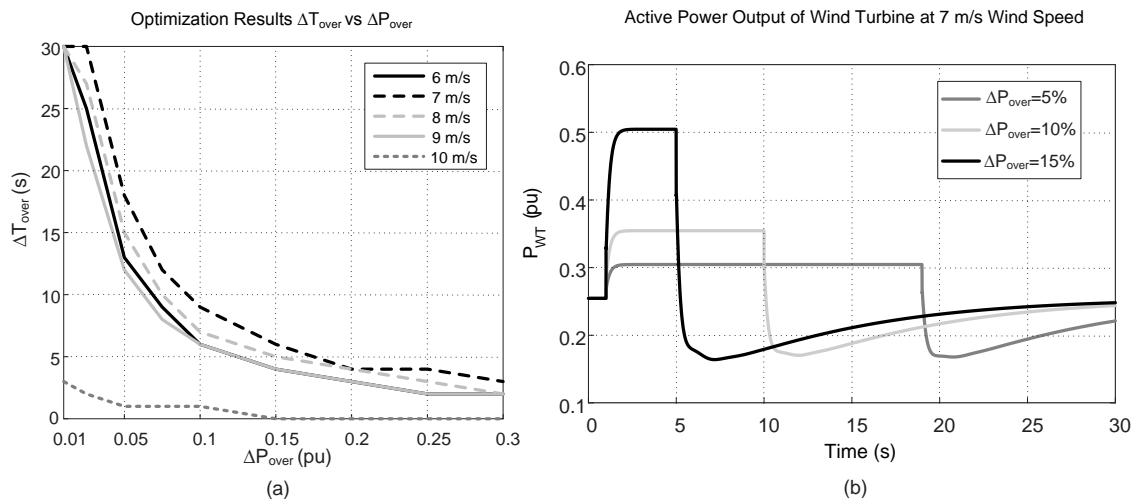


Figure 22. Optimization Results for Different Wind Speeds (a) and Active Power Output of Wind Turbine at 7 m/s Wind Speed

After conducting the optimization study for the fixed FFR control, the aeroelastic code HAWC2 is employed in order to analyze the impact of this FFR control on the structural loads. The HAWC2 is a Blade Element Momentum (BEM) based tool using a multi-body dynamics approach [23]. An open loop simulation is performed to run the HAWC2 and to obtain the loading of the structural components. For the open loop simulations, the baseline power controller in HAWC2 [24] is bypassed and the prescribed generator torque profile in time series is introduced as an input to the HAWC2 code in order to obtain different

overproduction power ( $\Delta P_{over} = 2.5\%$ ,  $10\%$ , and  $30\%$  of the available power) for different overproduction periods ( $\Delta T_{over} = 30\text{s}$ ,  $9\text{s}$ , and  $4\text{s}$ ), respectively. The results of the impact analysis are shown in Figure 23(a) in terms of active power performance and the calculated ultimate loads in Figure 23(b). Under the constant wind speed, especially the  $30\%$  overproduction case results in considerable increases in tower base, yaw bearing, and main bearing bending moments, mainly in the side-side/roll directions.

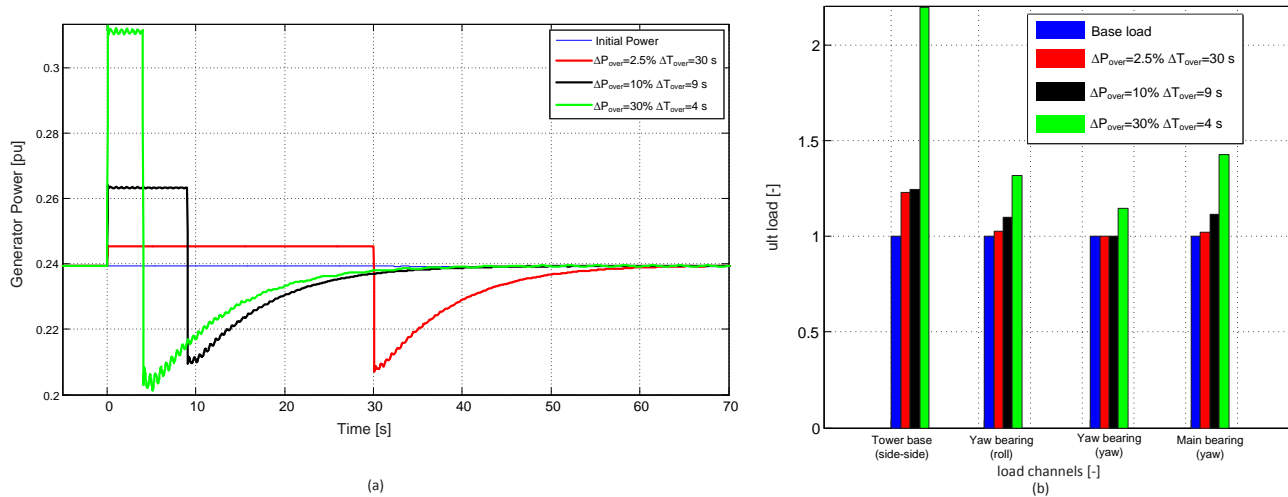


Figure 23. Structural Load Comparison at 7 m/s Wind Speed

In order to have primary frequency stability support from ReGen plants to ensure the system stability, these plants should have a resilient online coordination with the TSO (or the aggregator) which, however, depends on the requirements imposed on the ICT infrastructure. Latency, data rate, redundancy, serviceability, reliability, costs of deployment and ownership are factors that define the requirements and finally lead to a choice of technologies. Based on these communication technologies and network infrastructure, several test scenarios and cases can be introduced that may result in deviating primary frequency control performance in the distribution grid and thus, should be evaluated with respect to the related latencies and validity of the signals being exchanged between ReGen and the system operator (TSO)/Aggregator. The details of these test scenarios and cases will be documented in a standalone document that will comprehensively cover the ICT impact on primary frequency control coordination.

## 5 Frequency Restoration Reserve

### 5.1 Frequency Restoration Reserve (FRR) Control Principle

According to ENTSOE (European network of transmission system operators for electricity) [25], the framework of load frequency control includes three processes: frequency containment process, frequency restoration process and reserve replace process. In practice, this framework varies slightly in different synchronous area in terms of its implementation. For example [26], in Denmark, the western Denmark (called DK1, belonging to continental Europe synchronous area) and the eastern Denmark (called DK2, belonging to the Northern Europe synchronous area) have different frequency control manners. Namely, the main ancillary service products in DK1 for frequency control include FCR, FRR, and manual reserve, while the ancillary service products in DK2 include FCR, FRR, and manual reserve. Accordingly, the key

difference is that the service provider in DK1 responds to regulation signals sent by TSO, while the service provider in DK2 reacts to power system frequency. In detail, in DK1, the regulation signal is sent online as an output value from Energinet.dk (the Danish TSO) to each service provider with reference to the reserve bid, where the service provider must be able to maintain the regulation continuously; the frequency-controlled disturbance reserve in DK2 is activated automatically in the event of sudden frequency drops to under 49.9 Hz and remains active until balance has been restored or until regulation by means of the manual reserve takes over.

In this chapter, the secondary frequency control study is focused which is more suitable for ReGen's participation into the continental Europe synchronous area. However, considering ENTSOE's wish to harmonize the network code on load frequency control and reserves, it is likely that the secondary frequency control principle used in DK1 will also be implemented in DK2 in the near future. As discussed in [25] [26], two phases are needed for providing secondary frequency control: secondary reserve procurement phase and real-time operation phase.

- Secondary reserve could be procured daily, weekly or monthly in different power systems. In this study, it is assumed that the TSO buys the secondary reserve on a daily basis from service providers (e.g., balance responsible parties nowadays, aggregators in the near future power system), considering the increasing penetration of renewable energy resources which is hard to predict in a long term horizon. The secondary reserve consists of upward and downward regulation reserves which are requested as a combined, symmetrical reserve.
- In real-time operation, the secondary frequency control is automatic and provided by units which responds to regulation signals sent by Energinet.dk. The regulation signal is sent online every 4 seconds as an output value from Energinet.dk to each balance responsible party or aggregator in the near future. The regulation signal is normalized within  $[-1, 1]$  and the aggregator uses it with respect to the secondary reserve bids to provide the balancing power.

From the description above, it is indicated that the ReGen plants or aggregators who operate multiple ReGen plants need to submit secondary reserves to Energinet.dk day-ahead in order to provide secondary frequency control. It requires an economic trade-off design between spot energy market participation and frequency reserve market participation [27]. Nowadays, ReGen power plants are not allowed to participate in the reserve market because of the uncertainty in their power production. However, as the penetration of renewable energy resources increasing, it is necessary to consider ReGen plants as frequency service provider since they also have the capability to track power commands rapidly [28]–[30].

In real-time operation, achieving 100% performance accuracy when providing frequency regulation services is almost practically impossible, due to various reasons such as communications delays, measurement errors, control granularity, and unit's dynamics. For this reason, system operators define performance indexes, to assess the control performance. In general, service verification can be categorized in two main schemes.

- The first one is to pay as performance, e.g., implemented by PJM<sup>2</sup>, where each service provider is remunerated based on a number of performance criteria, one of which is the tracking accuracy [30].

---

<sup>2</sup> PJM is a regional transmission organization that coordinates the movement of wholesale electricity in all or parts of 13 states and the District of Columbia.

- The second is to establish performance requirements and maximum allowed errors, such as the performance index on secondary control by the Swiss TSO, Swissgrid [31]. Mainly, the control performance index of Swiss TSO will be used in this study to represent the applications of continental Europe synchronous area. The control performance index will be further detailed in section 5.3.1.

## 5.2 System architecture and assumptions

In this chapter, a statistical online decision system for aggregated ReGen power plants to provide secondary frequency regulation will be described. As shown in Figure 24, an aggregator level is proposed to coordinate the ReGen plants's power output in order to provide secondary frequency regulation services to transmission system operators (TSO). It is assumed that the reserve capacity  $P_{res}$  of each aggregator is symmetrical and at least being hourly constant throughout a period of 24 hours. Note that how to optimally make the day-ahead energy/reserve schedule of ReGen plants is not the focus of this study, the readers are referred to [27] for that purpose. The aggregator receives the normalized regulation signal  $r_t$  in  $[-1, 1]$  from the TSO every  $t_c$  seconds (e.g., 4 seconds in DK1). The aggregator must respond to  $r_t$  by providing power set points to each ReGen plant with respect to the planned reserve  $P_{res}$ . The power setting of aggregator is calculated based on a constant reference power  $P_{sch}$  sent to the TSO for a period of  $t_{sch}$  seconds, which corresponds to aggregator's output power for  $r_t = 0$ . We refer to each  $t_{sch}$  period as the scheduling period  $j$  (note  $j$  refers to a longer time period e.g. 10 mins, while  $t$  is the index used within the  $j$  time period), and the aggregator output must be regulated as

$$P_{agg,t} = P_{sch} + r_t P_{res} \quad (5.1)$$

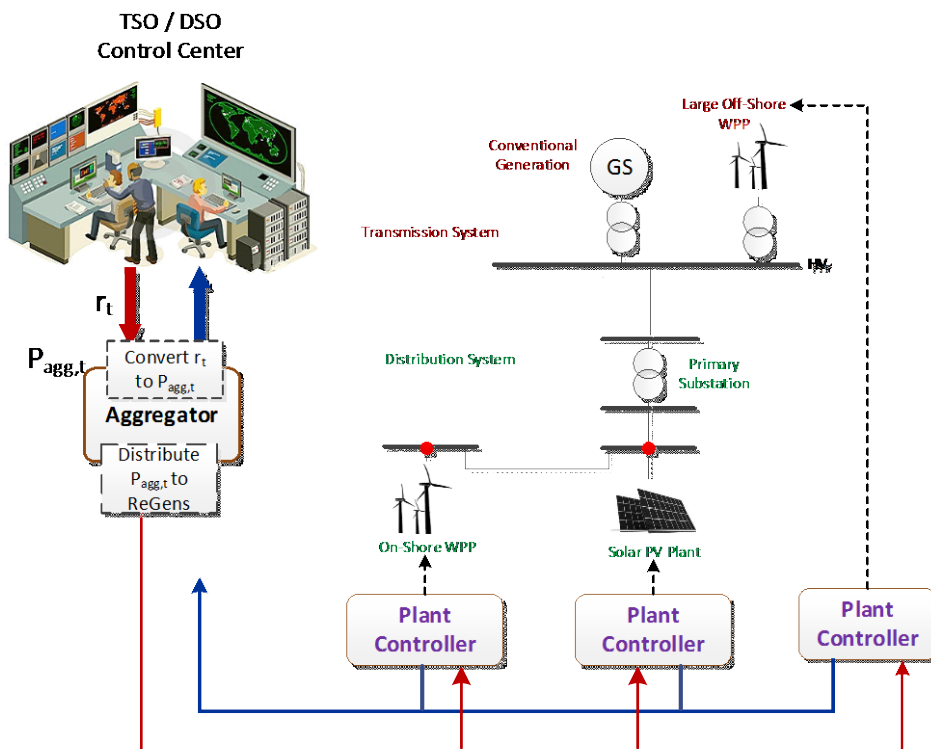


Figure 24: Overview of the system architecture

Since the regulation signal is sent every 4 seconds by the TSO, so in principle, the set point of  $P_{agg,t}$  could change every 4 seconds. How to distribute the  $P_{agg,t}$  to different ReGen plants in such a short time window is a research question. There are two approaches to dispatch the power set points to the ReGen plants belonging to an aggregator:

- One is a top-down centralized approach, namely, the aggregator calculates the  $P_{agg,t}$  every  $t_c$  and sets ReGen plants' operating point in a shorter time (less than  $t_c$ ) based on ReGen plants' real-time operational condition.
- Another approach is a bottom-up decentralized one, where a constant power and a reserve are pre-allocated to each ReGen plant for a pre-defined period of  $t_{sch}$  seconds, and then in real time, the aggregator passes the regulation signal  $r_t$  to every ReGen plant. Then, each ReGen plant calculates the power setting similar to the way presented in eq. 5.1, which will be further explained in section 5.3.4.

One can notice that the first approach has a high demand on the communication properties, which might not work for geographically distributed ReGen plants. The second approach is therefore investigated in this study, i.e., the aggregator aims to find the optimal power set point for each wind power plant  $P_{sch,t}^{WPP}$  and PV power plant  $P_{sch,t}^{PVPP}$ , respectively.

Next, the second approach is exemplified in the following for the case of a wind power plant (WPP). For example, by reducing its power output, a WPP can provide both upward and downward frequency regulation. We assume that the reserve capacity bidding was done in a robust manner, i.e. the WPP is able to fully meet the reserve provision requirements during all wind speed operating conditions. However, setting  $P_{sch,t_{sch}}$  so that any  $r_t$  can be followed under different possible wind power scenarios is a very conservative approach, which can lead to curtailing large amounts of wind power. Figure 25 shows how  $P_{sch,t_{sch}}$  would be chosen given the 10 mins wind power scenario, so that any  $r_t$  would be followed at every time step. Note that the wind power shown in the figure is an example. It is also reasonable to assume that near-to-second prediction of the wind speed for a period of 5-10 minutes is unrealistic, therefore wind-speed uncertainty must also be considered. Under a robust short-term scheduling,  $P_{sch,t}$  would be chosen by considering the worst-case realization of the wind speed, leading to a very conservative scheduling.

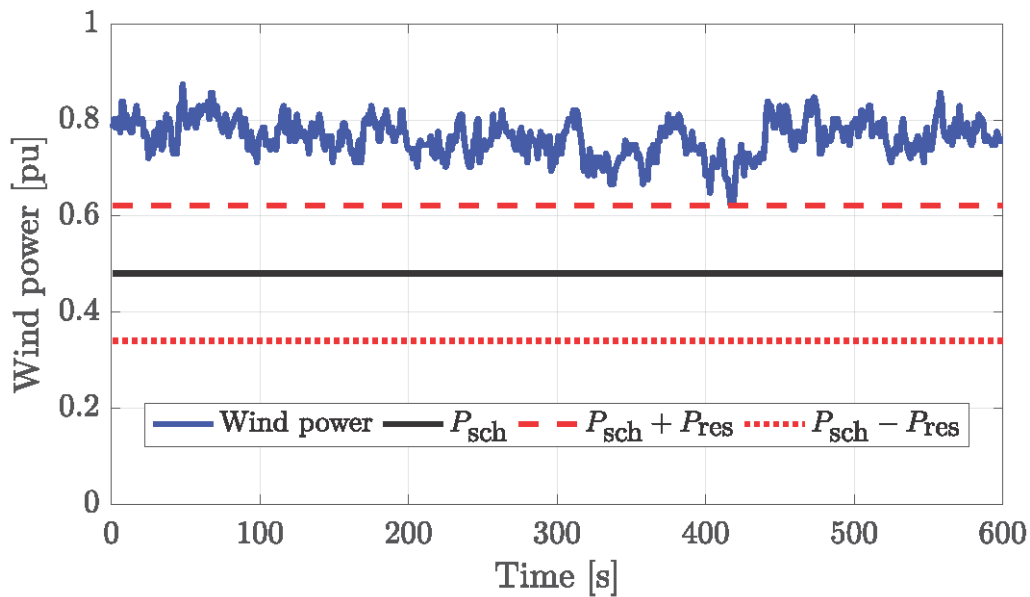


Figure 25: Short-term scheduling of a WPP for robust service provision

A statistically-based short-term aggregator online decision system, which utilizes the statistical properties of the secondary frequency regulation signal, e.g., one can try to quantify a probability where the activated reserve only uses 50% or less of the full reserve bid, the control performance margin of the provided service and the statistical non-coincidence of wind speed/solar irradiance, is proposed in the following. Such a scheduling method can be used by the aggregator to choose the  $P_{sch,t_{sch}}$  which optimizes its profits, for instance to minimize the imbalance cost due to the difference between  $P_{sch,t_{sch}}$  and the day-ahead schedule or to minimize wind/PV-power curtailment. Without loss of generality, this approach will be used to study the potential reduction in wind/PV-power curtailment, while meeting the service provision requirements.

Considering all these factors, the assumptions and system setup can be summarized as follows:

- At every scheduling period  $j$ , the aggregator calculates the maximum  $P_{sch}$  for the following  $t_{sch}$  second, while respecting the service requirements.
- Due to the small frequency control time steps (in the order of 2 to 4 seconds) and the relatively small power changes, fast WPP dynamics are neglected.
- $P_{res}$  is known and has been set in a robust manner, guaranteeing full service delivery at the worst case.
- The aggregator predicts the wind/PV power for the following  $t_{sch}$  second. In this study the perfect forecast of the average wind speed/solar irradiance for each minute is assumed, with an added Gaussian noise, whose properties are calculated from historical wind data/solar irradiance.
- The regulation signal is sent every  $t_c$  seconds. Note that how the TSO generates the regulation signal is not investigated in this report, i.e., the control system is an open loop. However, the control method can handle multiple regulation signals, i.e., the aggregators can track different power settings.

### 5.3 Statistical control method

In this study, a statistical but generic method for aggregated ReGen plants to provide secondary frequency regulation is presented. The statistical method uses the historical frequency regulation signal to optimize the power set point of individual ReGen plant based on the very short-term predicted wind/pv power and the secondary frequency control (SFC) control performance requirements of ENTSOE [31].

#### 5.3.1 Control performance index

In the case of Swissgrid [31], the pre-qualification process requires a minimum accuracy of 1%, calculated by the following formula

$$\frac{\sum_{t=1}^{t_{tot}} |P_{diff,t}| t_c}{P_{sec} t_{tot}} \cdot 100\% \leq 1\% \quad (5.2)$$

As illustrated in Figure 26,  $P_{sec}$  is two times of the reserve  $P_{res}$ ,  $P_{diff}$  is the power value in excess of the tracking tolerance which is equal to  $1.25\% P_{res}$  around the power reference, and  $t_{tot}$  is the total test time, i.e., 75 mins in the Figure 26. This formula will be used in our study to calculate the control error every 10 mins over a horizon, e.g., 24 hours. From the equation, it is noted that the error is calculated over the period.

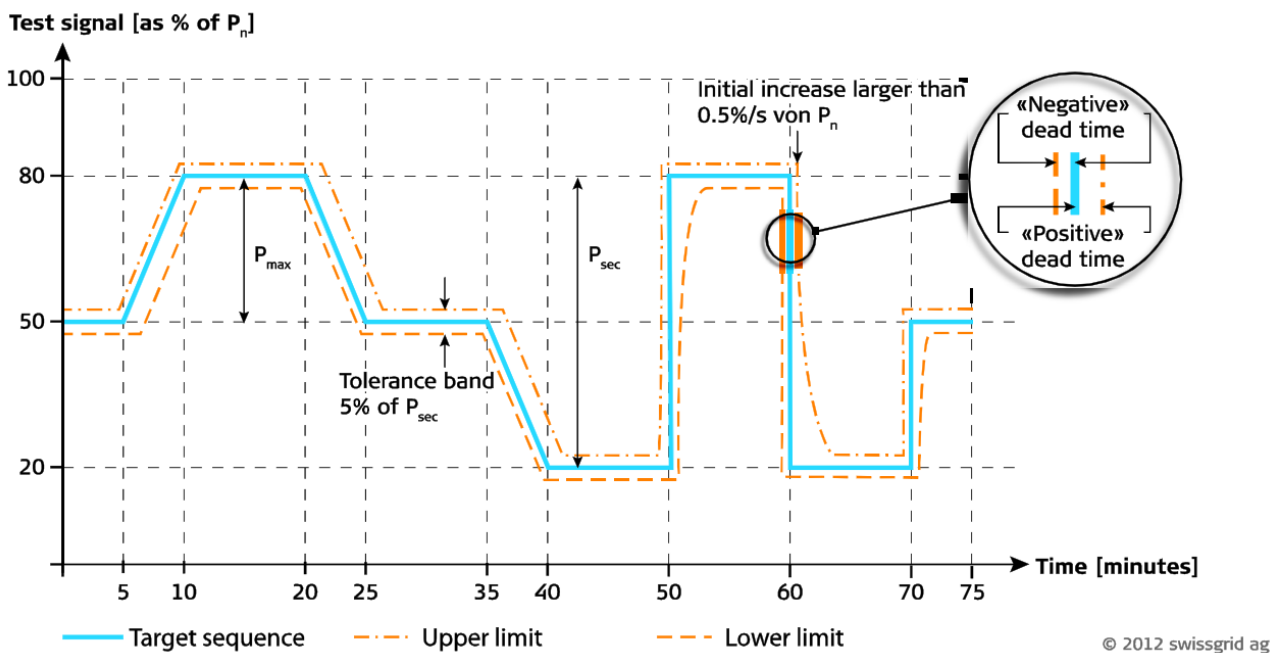


Figure 26: Test signal with tolerance band [29]

#### 5.3.2 Wind and PV power uncertainty modeling

The wind power at the plant level is approximately estimated and calculated from the following formula [32] where equivalent wind speed of a wind plant is used as inputs:

$$P = \begin{cases} 0 & \text{if } V \leq V_{in} \text{ or } V \geq V_{out} \\ \frac{V - V_{in}}{V_r - V_{in}} P_N & \text{if } V_{in} \leq V \leq V_r \\ P_N & \text{if } V_r \leq V \leq V_{out} \end{cases}$$

where  $V, V_{in}, V_r, V_{out}$  are the wind speed, cut-in speed, rated speed, and cut-out speed respectively.  $P$  represents the available power, and  $P_N$  denotes the rated power.

As described in Section 5.2, it is assumed that the average 10 minutes wind power over a period of  $t_{sch}$  seconds can be perfectly predicted. Based on available historical data, we observed that the per-second variation of wind power around the 10 minutes average value is normally distributed. Moreover, we observed a strong autocorrelation of the variation, as is evident in Figure 27 for a random wind scenario. In this study, we randomly select the wind power variation from the historical samples and then add them on top of the predicted 10 minutes based wind power.

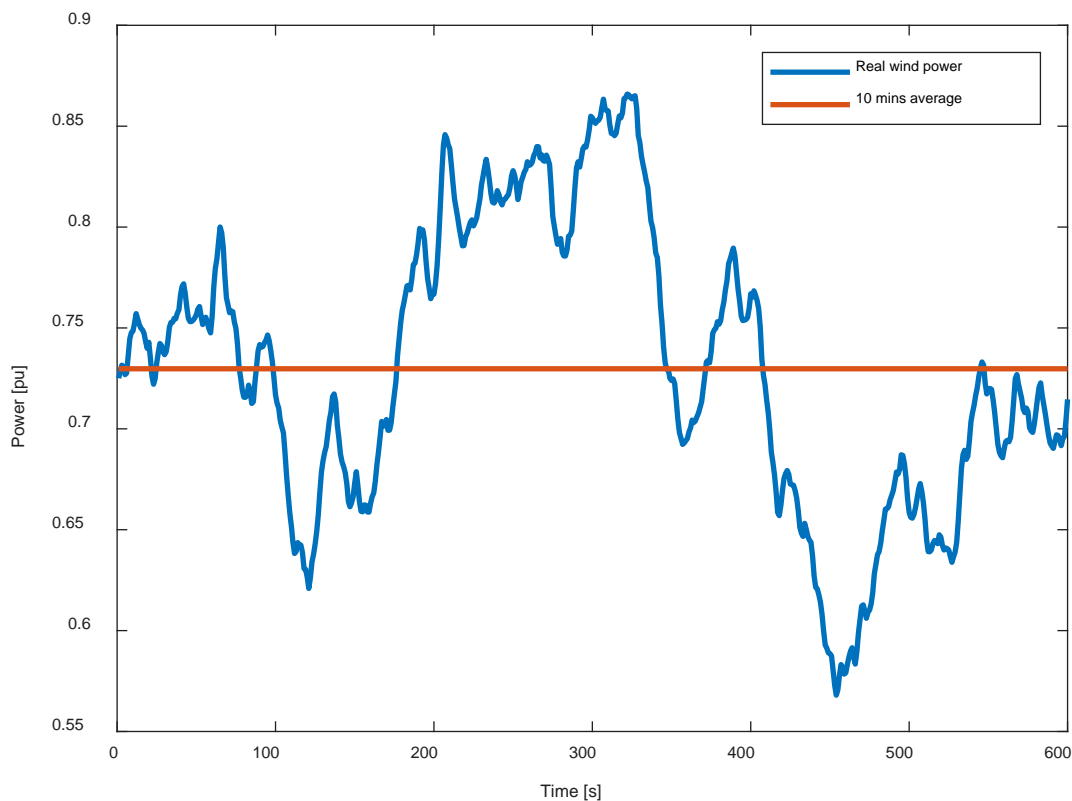


Figure 27: Short-term output power and 1 min average power of a WPP

Similarly, we can also calculate and predict the PV power over a period of  $t_{sch}$ , e.g., according to [9].

### 5.3.3 Statistical online decision system

With the estimated wind/PV power scenarios for each plant, the aggregator will choose the power schedule  $P_{sch}$  of each ReGen for the following  $t_{sch}$  control period, in order to provide the committed reserve capacity  $P_{res}$  within the service performance margin. In our example a robust day-ahead commitment is assumed, and the aggregator tries to reduce the wind curtailment. As shown in Figure 28, the aggregator online decision making system updates the base power setting  $P_{sch}$  every 10 minutes. The aggregator online decision system relies on several inputs including the historical regulation signal samples, the daily defined energy/reserve schedule, the very-short term wind power forecast and scenario generations, as well as the control performance index. Note that:

- For the amounts of the historical regulation samples, the selection of an optimal number of samples needs some preliminary studies, e.g., a small size of samples but can potentially characterize all the features of the regulation signal, e.g., one month sample of regulation signals can represent the main features of a year regulation signals. This is not the focus of this study, but can be approached in the near future;
- For the daily defined energy/reserve schedule, as discussed in Section 1, readers should refer to [27] for quantifying the optimal allocation;
- The forecast is described in Section 5.3.2;
- In terms of the control performance index, as described in Section 5.3.1, the control error is calculated over a period, which means the control performance index can be dynamically modified overall the whole schedule period, e.g., 24 hours in every 10 mins. One can imagine that the aggregator can have a better prediction if the wind blow steadily in the day time, thus, the control error could be smaller in these periods. The situation implies that the control error could be relaxed a bit in other time slots, given the fact that the overall control error will be kept less than 1% in a 24 hours horizon. This idea can be described systematically by using the budget concept developed in [34], which is an interesting research direction. The budget concept means that if a control performance index is set for one day operation, the online decision system can adaptively modify the 10 mins-based control performance index based on the control performance of the realized time slots. Next, we will describe the algorithms used in the online decision system.

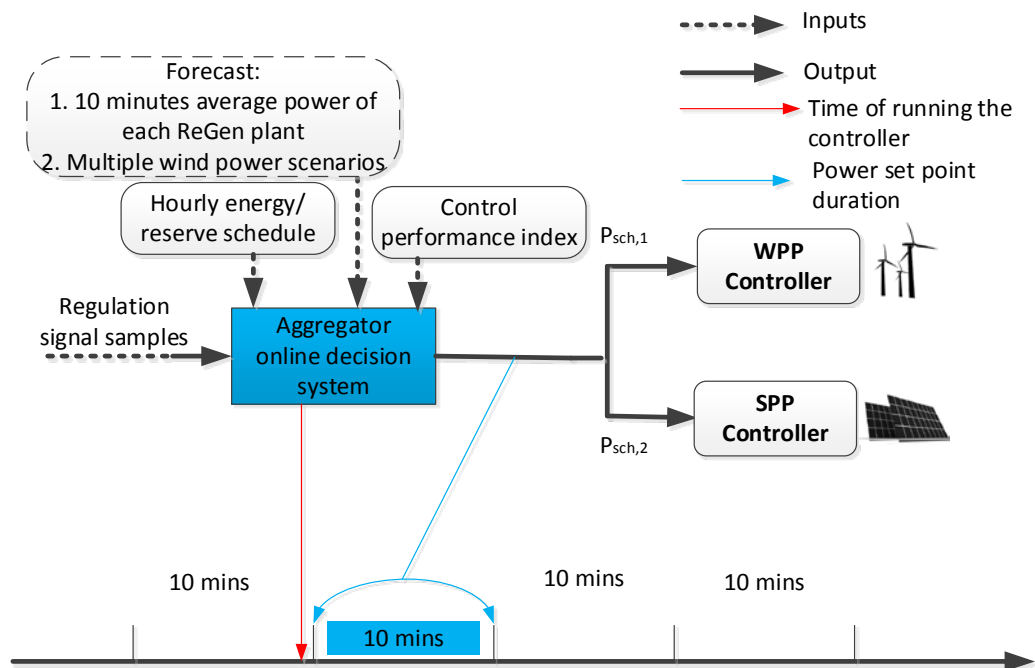


Figure 28: The online decision system of aggregator for generating the base power  $P_{sch}$  every 10 minutes

To illustrate the statistical online decision system, we start with the case where the aggregator controls only one WPP. Then, we will extend the method to the case of more than one WPP/SPP. In either case, the control principle is to increase the value of  $P_{sch}$  while fulfilling the control performance requirement as described in section 5.3.1. To derive this value  $P_{sch}$ , a statistical analysis is performed where the following parameters are used:

- Multiple wind/PV power scenarios, e.g.,  $N$  scenarios, as indicated in point 2 of the 'Forecast' block of Figure 28. To predict the multiple wind/PV power scenarios, one could refer to [35][36]. Here, we use the historical variation samples to obtain the multiple power scenarios.
- Various historical regulation signal samples, e.g.,  $M$  samples, as shown in the left part of the figure.

The statistical control method starts from the minimum value ( $P_{sch}$ ) of the base power ( $P_{sch}$ ) and then the value is increased step by step, being limited by a maximum step number  $D$ . For each value of the base power  $P_{sch}$ , it will experience  $N$  wind/PV power scenarios. In each wind/PV power scenario, the  $M$  regulation signals will be used to evaluate the control performance. The control error is calculated and assessed based on (5.2). In total, a number of  $N * M * D$  errors will be generated. Afterwards, these errors will be analyzed and the largest value of  $P_{sch}$  that has error less than 1% will be selected as the power setting point for the ReGen plant. At the end of the statistical analysis, the aggregator online decision system is able to quantify an approximated error as a function of the base power  $P_{sch}$ . This function comes from fitting an exponential curve in a form of  $\delta = a * e^{b * P_{sch}}$ , where  $a, b$  are parameters that need to be quantified.

In terms of the case of having multiple ReGen plants within one aggregator, one can apply the similar method to calculate the control error of an aggregator whose power consists of different ReGen plants. We will elaborate this via case studies in section 5.4.

After obtaining the  $P_{sch,i}$  for the coming 10 mins, these solutions will be used by the aggregator to perform the real time control. The real time controller is described in the following section.

### 5.3.4 Aggregator real-time controller

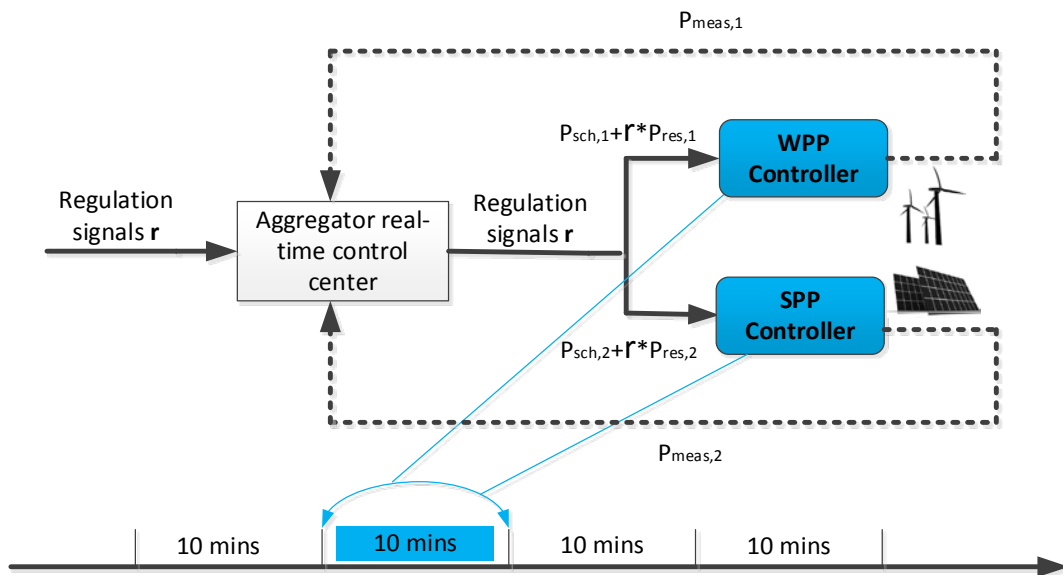


Figure 29: Real-time control operation

As indicated in Figure 29, in real-time operation, the aggregator receives the regulation signal from the TSO and sends it to each ReGen plant. After receiving the regulation signal, each ReGen plant calculates the power set point. Note the control system is an open loop; however, the power measurement of each ReGen plant is needed to quantify the control error as well as to redefine the control performance index

(see discussions in Section 5.3.3). Note that real time control operation is not the focus of this report, instead, verification of the proposed method for real-time operation will be reported in Replan Project WP5 deliverables.

## 5.4 Case studies

### 5.4.1 Two wind power plants

A set of real wind speed measurements as well as historical regulation signals are used to illustrate the proposed statistical control method. For the wind power calculation, the cut-in speed, rated speed and cut-off speed are 3 m/s, 13 m/s, and 25 m/s, respectively. Power is expressed per MW per ReGen. In the simulation, relevant parameters of the two wind power plants are listed/assumed as follows:

- Nominal power capacity of WPP1 and WPP2 are 15 MW and 30 MW, respectively; note that the available second-based wind speed at wind plant level is a real measurement, but the size of the two WPP plants are assumed here.
- 10 minutes mean power of WPP1 and WPP2 are 0.7298 pu and 0.6796 pu, corresponding to 10.9470 MW and 20.3880 MW, respectively;
- Reserve power of WPP1 and WPP2 are 20% of the mean power, which equal to 2.1893 MW and 4.0778 MW, respectively;
- The step increment power of WPP1 and WPP2 are 0.01 pu of the nominal power, corresponding to 0.15 MW and 0.3 MW, respectively.

As discussed, in real time, the control purpose is to increase the  $P_{sch}$ , i.e., to increase the bulk power supply and meanwhile ensure safely the reserve capacity. Figure 30 shows 20 possible predicted wind power scenarios as well as the minimum  $P_{sch}$  (pu, normalized per WPP plant). With this setup, the power value of  $P_{sch}$  is 0.3513 pu (5.2695 MW) and thus it is not economically optimal for the aggregator.

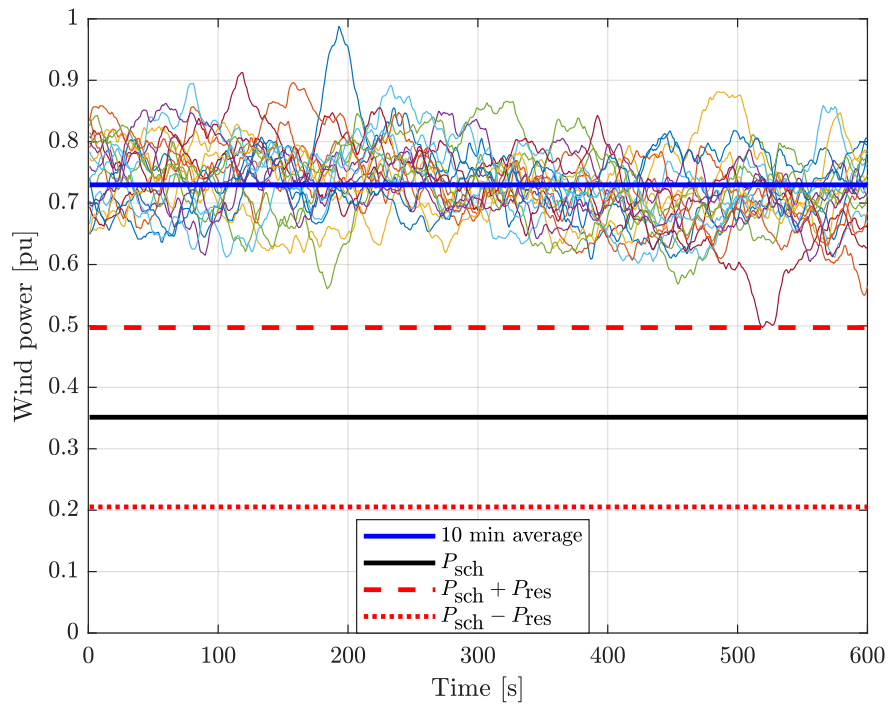


Figure 30: 10 minutes power of WPP1 with multiple scenarios. The black line represents the robust scheduled power, the red lines show provided reserve, the blue line shows the predicted 1 min average wind power, and the other colored lines show 20 possible wind power scenarios.

Similarly, we also show the same power values for WPP2 in the Figure 31.

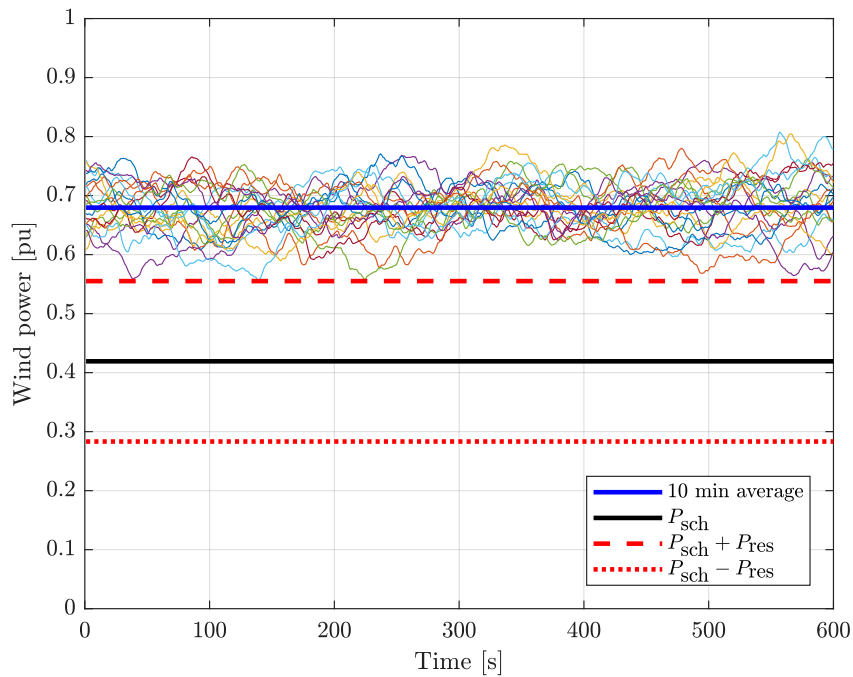


Figure 31. 10 minutes power of WPP2 with multiple scenarios. The black line represents the robust scheduled power, the red lines show provided reserve, the blue line shows the predicted 1 min average wind power, and the other colored lines show 20 possible wind power scenarios.

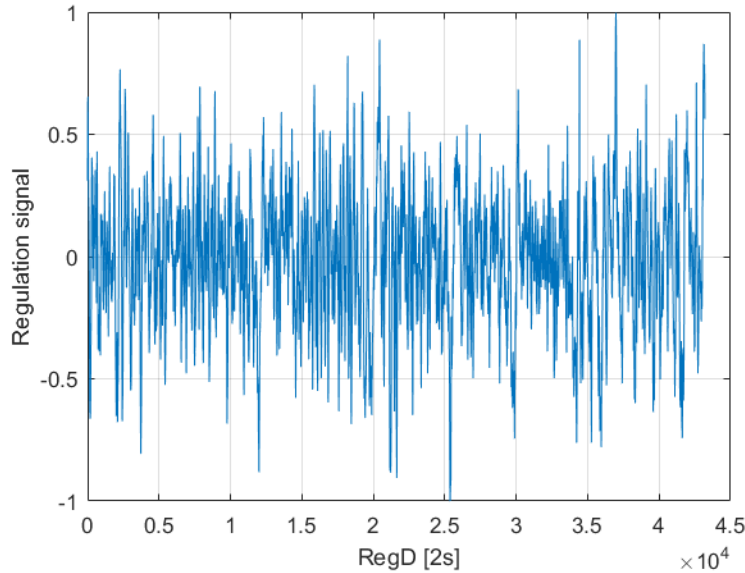


Figure 32: One day example of the RegD regulation signal

In terms of the regulation signal, RegD signal of PJM as one type of regulation signals  $r_t$  is used and the data is available online. (We use this data as a SFC signal because SFC data from the ENTSOE area was not publicly available; thus the RegD signal is used since the regulation signals used in PJM and ENTSOE area share similarities.) In PJM market, two types of frequency regulation signals  $r_t$  are used: RegA stands for regulation A, traditional regulation, RegD stands for regulation D, dynamic regulation. These two signals works together to optimally control area control error. The RegA is mainly used to regulate the power output of big power plants, while RegD is mainly designed for small units who can respond to the regulation signal very fast. As presented in [30], RegD is more favorable by renewable power plants. Thus, RegD signal is used in our study. Figure 32 shows an example of one-day RegD signal. Note the RegD signal is sent every 2 seconds in PJM market (in Denmark, the signal is sent every 4 seconds). This means there are 300 regulation signals in every 10 mins. We selected 1000 samples historical RegD signals for the simulation. Each sample contains 300 values.

We will start with individual WPP error calculation, with the inputs described above; we start from the minimum value of the base power  $P_{sch}$  and add all the regulation signals on top of the base power, so we will have 1000 possible power setting during the ten minutes. Then, we test these power settings with the 20 possible wind power scenarios. Afterwards, we increase the base power per step by 0.01 pu. With the new value of the base power, we repeat the simulation. Overall, at the end, we will get  $20 \cdot 30 \cdot 1000$  errors calculated. The simulation takes around 4 seconds, which is performed in Matlab version 2016a with a central processing unit of Intel Core i7, 2.60GHz. By looking into the errors, we quantify the base power value of each wind power scenario that can optimally provide the secondary frequency control. Figure 33 shows the control error of each wind power scenario versus the base power. From which, one can derive the mean control error as a function of the base power setting, assuming that these wind scenarios have the same probability. The red curve in the Figure 33 is the mean error of WPP1 given the increasing power

setting. From the curve, the aggregator is able to quantify that power setting of 9.62 MW of WPP1 makes the expected mean error around 1%.

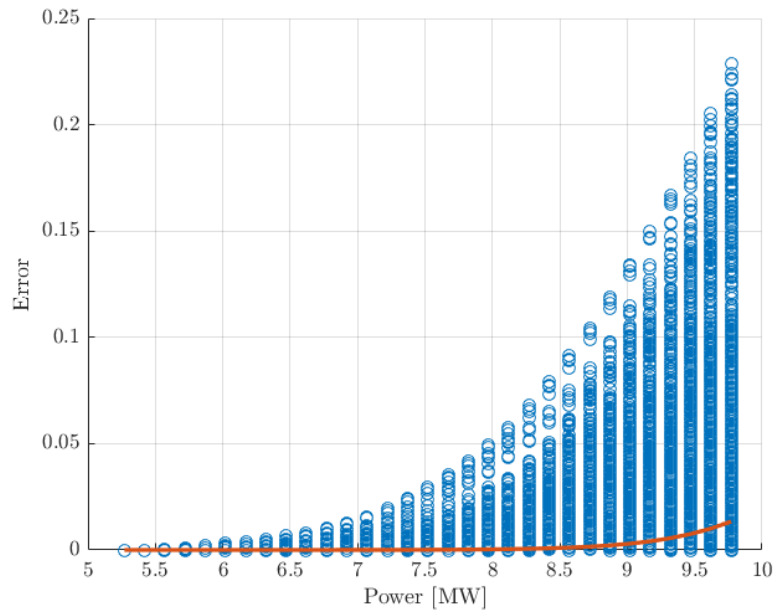


Figure 33: WPP1 Control error versus base power  $P_{sch,1}$

Similarly, we also get the control error curve for WPP2 and from which, the aggregator is able to quantify that power setting of 18.34 MW makes the expected mean error around 1%.

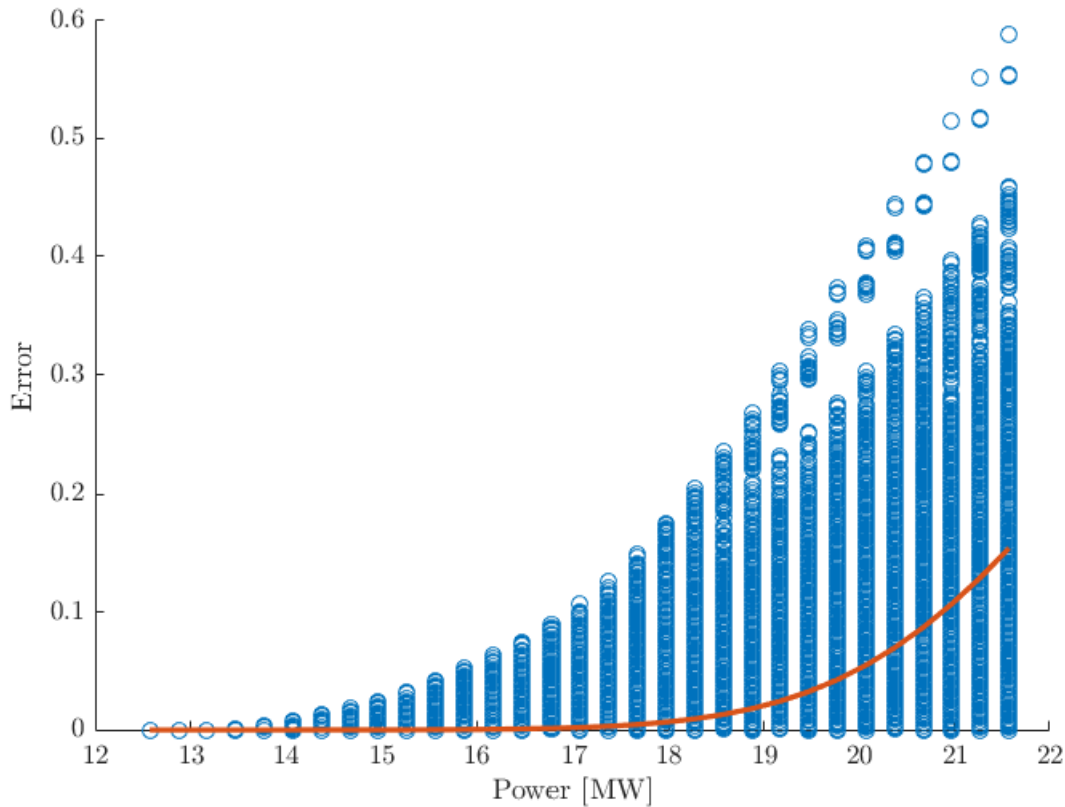


Figure 34. WPP2 Control error versus base power  $P_{sch,2}$

Next, we will present the mean expected error by combining different power setting of WPP1 and WPP2. As shown in Figure 35, the aggregator can use different combination of WPP1 and WPP2 that makes the error less than 1%. It is observed that power setting 8.8705 MW of WPP1 and power setting 19.7740 of WPP2 makes the expected mean error of aggregator around 1%. The aggregate power of the aggregator is 28.6445 MW which exceeds the sum of the power of WPP1 (9.62 MW) and WPP2 (18.34 MW) obtained previously, if WPP1 and WPP2 are handled individually. Furthermore, with the curve, it is possible for the aggregator to quickly modify each WPP’s power setting in the real time depending on the working condition of WPPs.

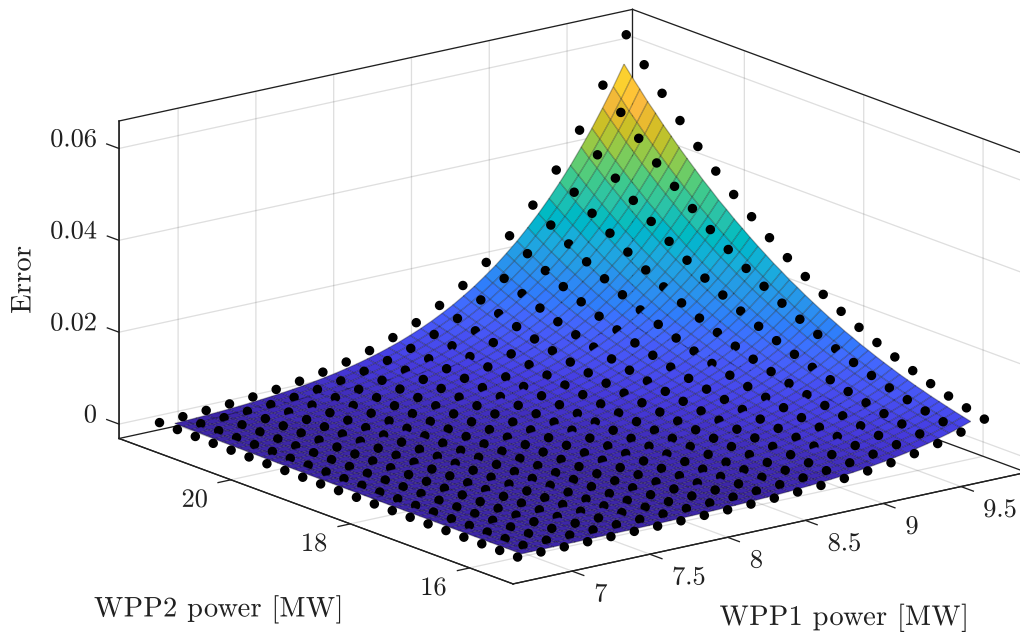


Figure 35 Expected mean error of aggregator versus power setting of WPP1 and WPP2

#### 5.4.2 Three PV plants

In this study, the proposed method is also tested on the three PV plant of SYSLAB located in DTU Risø campus<sup>3</sup>. The SYSLAB facility is spread across multiple locations around the former wind turbine testing site, making use of Risø's spacious premises. Its backbone is formed by a 400V grid with six busbars at three substations. A central crossbar switch with tap-changing is allowing meshed operation and power flow control. Three PV plant is connected to the SYSLAB power system at three sites (building 117, 319, 715) distributed over 1 km. The SYSLAB monitoring system measures the power for each PV installation and the aggregated power at the grid connection with a time resolution of 1 sec. Meanwhile, solar irradiation, temperature, and wind speed nearby the three PV plants are also measured and thus make it suitable for aggregator to control.

<sup>3</sup> <http://www.powerlab.dk/Facilities/SysLab>



Figure 36: One PV plant located near building 715

The three PV plant have different power profiles during the day due to their different orientations and tilt-angles. The nominal power of PV plant at 117, 391 and 715 are 10 kW, 10 kW, 7 kW, respectively. In the simulation, 10 mins average power of PV 117, PV 319, and PV 715 are 7 kW, 6kW, and 4 kW, respectively. It is assumed the 20% of the 10 mins average power will be used for reserve. The step increment powers of three PV plants are 0.01 pu of the nominal power. With the same frequency regulation signal samples and the tolerance calculation method, one could get three error curves individually, if only one PV plant is used by the aggregator one time. From the following curves, the aggregator can quantify the power setting that makes the expected mean error less than 1%.

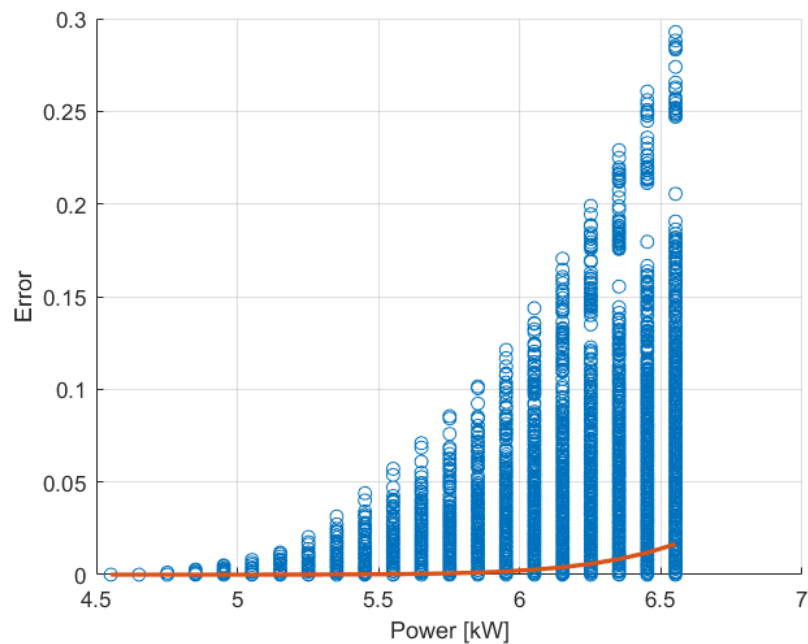


Figure 37: PV117 Control error versus base power setting

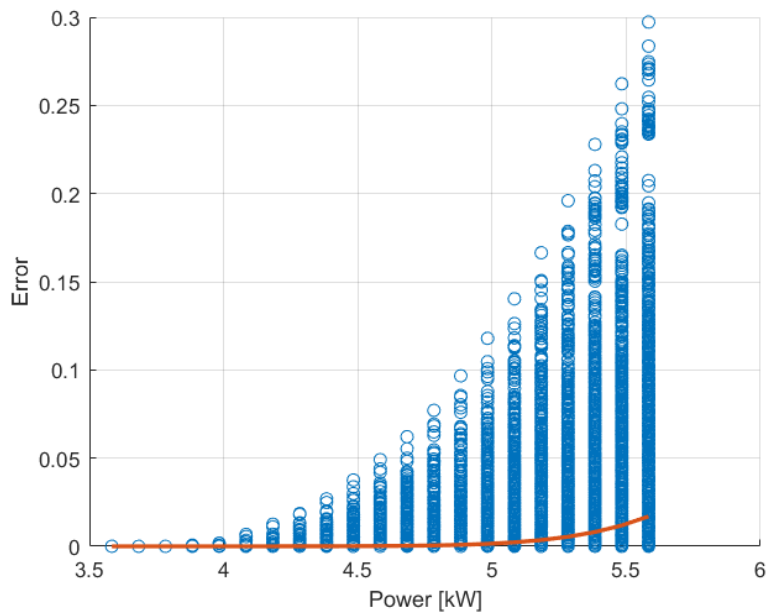


Figure 38: PV319 Control error versus base power setting

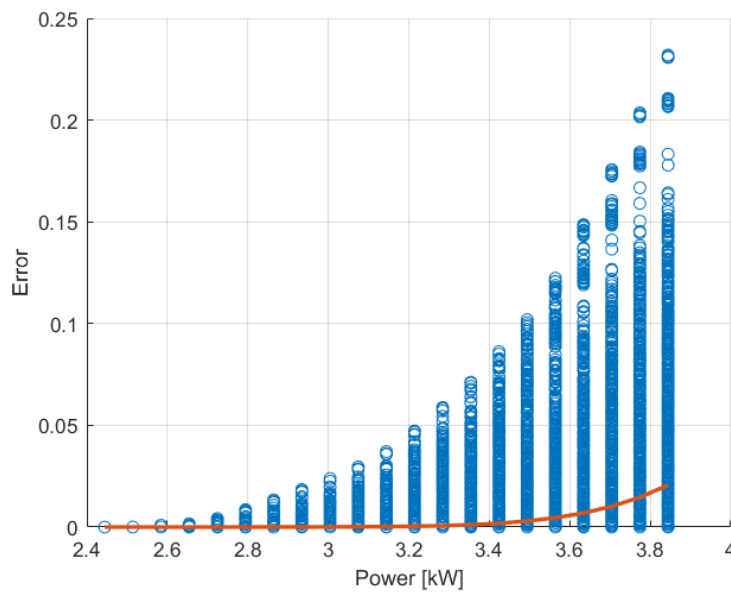


Figure 39: PV715 Control error versus base power setting

Furthermore, a relation between the expected mean control error and all possible combination of three PV plants power setting is also obtained. Note that it is not easy to visualize the relation between the errors and three power settings of PV plants. In terms of the way to pick the right power setting combinations, it is suggested that the aggregator could fix one PV plant power setting first, then select the optimal combinations of other two PV plants. Similarly, the method is applicable to other cases where aggregator has more ReGen plants.

## 5.5 Discussion

Note that the study uses several assumptions which need to be considered and improved in practice, for example, prediction errors of the 10 mins-based power from the day-ahead prediction to the near real time power output is not considered. We assume that the day-ahead predicted mean ReGen available power still holds when it is close to real time. Therefore, we only need to focus on near real time operation, i.e., try to increase the base power setting of ReGen plants. This prediction error (from DA to near real time) should be considered in the future work. In addition, the used 20 wind power scenarios may have different probability; this will influence the aggregated error function. In the future work, these factors will be considered. Furthermore, we plan to validate the proposed control method with the PJM RegA signal which has different features comparing to PJM RegD signal. In addition, we plan to observe the control performance of the ReGen plants by considering other factors such as communication delays.

## 6 Summary

The economic and technical benefits of having ReGen power plants as a frequency service provider makes the research topic getting higher attention recently, even though there is a big concern regarding ReGen power plant's fluctuating power output.

In the fast frequency response part, an optimization approach is developed in the TSO level to coordinate the FFR of WPPs. By using the results of the optimization study have shown that it is possible to improve the frequency nadir in the majority of the considered scenarios. The coordination depends on the available power of each WPP and the wind power penetration level. Accordingly, the response of WPPs can be coordinated by enabling the WPPs with high wind first and then using the WPPs with low and medium wind speed conditions. From the simulation results, it has been seen that in scenarios with a large amount of wind generation operating at medium wind speeds, some WPPs have been dispatched to react not on the initial frequency drop but on the second dip caused by the frequency support of the other WPPs. In that way, it has been possible to alleviate the severity of the second dip. Furthermore, the overproduction of the WT capability is investigated. According to the results of this investigation, the maximum energy can be extracted depending on the overproduction power setpoint, the duration of the overproduction, and the operating conditions of the wind turbine for different wind speeds. Additionally, it is seen that for different wind turbine sizes, the optimum energy is released around the same wind speed region. Looking at the impact of the short-term overproduction on the wind turbine loading, it has been seen that the ramp down rate of the active power after the overproduction is crucial for the structural loading.

Regarding frequency restoration reserve, a statistical online decision making system is proposed that can optimally allocate base power setting to ReGen power plants in terms of :a) the power setpoints of ReGen power plants can be significantly increased, compared to a conservative setting, and b) its capability to track the secondary frequency regulation signal. As a result, the proposed method can improve the economics of the ReGen power plant and meanwhile respecting the frequency service performance requirement. The method uses a statistical approach to quantify the base power setting that makes the expected mean control error less than 1%. This 1% control error is allowed by the TSO. The method considers multiple wind power scenarios and various possible regulation signals. The two case studies of wind power plants and PV power plants show that the base power setting can be increased significantly compared to the most conservative setting.

In summary, ReGen power plants are capable to provide secondary frequency control, given the abundant available renewable power. To make the control a success, it is recommended that:

- With a better ReGen power scenarios prediction error, the on line decision system can give better decisions;
- If the aggregator has more ReGen power plants, it is recommended to keep the predicted ReGen power scenarios small, since the online decision system needs to take more computational time to compute the control error of all ReGen power plant setting combinations;
- When constructing the ReGen power scenarios, correlations between different ReGen power plant's power output could be considered which give a more accurate power scenario input to the online decision system;
- To control the ReGen power plants power output, 10 mins time window is selected here, but this interval can be modified depends on the ReGen power output prediction accuracy;
- Instead of using expected mean error index, the aggregator may use other error index to quantify the base power, such as percentile-based value.

## 7 References

- [1] ENTSO-E, "Future System Inertia Report," Energinet, Svenska kraftnät, Statnett, Fingrid (Nordic Analysis Group).
- [2] Wall P, Shams N, Terzija V, Hamidi V, Grant C, Wilson D et al. "Smart frequency control for the future GB power system," IEEE PES ISGT Europe, 2016.
- [3] Energinet, Technical regulation 3.2.5 for wind power plants above 11 kW, 22.07.2016.
- [4] Energinet, Technical regulation 3.2.2 for PV power plants above 11 kW, 14.07.2016.
- [5] ENTSO-E, Commission Regulation (EU) 2016/631 establishing a network code on requirements for grid connection of generators, 14.04.2016.
- [6] ENTSO-E, Need for synthetic inertia (SI) for frequency regulation, guidance documents for national implementation for network codes on grid connection, 29.03.2017.
- [7] Sharma S., Huang S. and Sarma N.. System inertial frequency response estimation and impact of renewable resources in ERCOT interconnection. IEEE PES General Meeting, San Diego, CA, 2011.
- [8] ERCOT, "Future Ancillary Services in ERCOT," Jan. 2013.
- [9] Hydro-Quebec TransEnergie, "Transmission Provider Technical Requirements for the Connection of Power Plants to the Hydro –Quebec Transmission System," Feb. 2009
- [10] Brisebois, J.; Aubut, N., Wind farm inertia emulation to fulfill Hydro-Québec's specific need. Power and Energy Society General Meeting, 2011, Pages: 1 - 7, DOI: 10.1109/PES.2011.6039121
- [11] National Grid UK, "GB System Operability Framework," Sept. 2014.
- [12] G. C. Tarnowski, "Coordinated Frequency Control of Wind Turbines in Power Systems with High Wind Power Penetration," Technical University of Denmark, Lyngby, PhD thesis, 2011.
- [13] Gowaid, I. A., El-Zawawi A., El-Gammal M., Improved Inertia and Frequency Support from Grid-Connected DFIG Wind Farms, IEEE Power and Energy Society General Meeting 2011
- [14] Brisebois, J.; Aubut, N., Wind farm inertia emulation to fulfill Hydro-Québec's specific need. Power and Energy Society General Meeting, 2011, Pages: 1 - 7, DOI: 10.1109/PES.2011.6039121
- [15] Müfit A., "Dynamic Frequency Response of Wind Power Plants", PhD Thesis, Aalborg University, Aalborg, Denmark, 2012.

- [16] Hansen A.D., Altin M., Iov F., “Provision of enhanced ancillary services from wind power plants – examples and challenges” *Renewable Energy Journal*, nr. 97, 2016, pp. 8-18.
- [17] Hansen A.D., Altin M., “Impact of advanced wind power ancillary services on power system “ 2014 report DTU Wind Energy E-0081, ISBN 978-87-93278-26-4
- [18] M. Asmine, C.-E. Langlois, “Field Measurement for the Assessment of Inertial rEsponse for Wind Power Plants based on Hydro-Quebec TransEnergie Requirements,” 13th International Workshop on Large-Scale Integration of Wind Power into Power Systems as well as on Transmission Networks for Offshore Wind Farms, Oct. 2014 Berlin, Germany.
- [19] J. Machowski, J. W. Bialek, J. R. Bumby, *Power System Dynamics: Stability and Control*. John Wiley & Sons, Ltd., 2008.
- [20] Kaushik Das, “Integration of Renewable Generation in Power System Defence Plans,” PhD Thesis, 2016.
- [21] ENTSO-E, “Final Report System Disturbance on 4 November 2006,” 30.01.2007.
- [22] Mathworks. (2017). *Global Optimization Toolbox: Genetic Algorithm*, [Online]. Available: <https://se.mathworks.com/help/gads/genetic-algorithm.html>
- [23] T. J. Larsen et al. *How 2 Hawc2, the user’s manual Technical report, Risø-R-1597(ver. 4-4) (EN) 2013.*
- [24] DTU Wind Energy Controller, <https://github.com/DTUWindEnergy/BasicDTUController>.
- [25] European Network of Transmission System Operators for Electricity, “Supporting document for the network code on load-frequency control and reserves,” 2013.
- [26] Energinet.dk, “Ancillary services to be delivered in Denmark Tender conditions,” no. 8871/11, p. 49, 2012.
- [27] T. Soares, P. Pinson, T. V. Jensen, and H. Morais, “Optimal offering strategies for wind power in energy and primary reserve markets,” *IEEE Trans. Sustain. Energy*, vol. 7, no. 3, pp. 1036–1045, 2016.
- [28] J. Aho, A. Buckspan, L. Y. Pao, and P. A. Fleming, “An Active Power Control System for Wind Turbines Capable of Primary and Secondary Frequency Control for Supporting Grid Reliability,” *AIAA/ASME Wind Symp.*, no. January, pp. 1–13, 2013.
- [29] C. R. Shapiro, J. Meyers, C. Meneveau, and D. F. Gayme, “Wind farms providing secondary frequency regulation: Evaluating the performance of model-based receding horizon control,” *J. Phys. Conf. Ser.*, vol. 753, p. 52012, 2016.
- [30] J. Aho, L. Y. Pao, P. Fleming, and E. Ela, “Controlling Wind Turbines for Secondary Frequency Regulation : An Analysis of AGC Capabilities Under New Performance Based Compensation Policy,” *13th Wind Integr. Work.*, no. February 2015, 2014.
- [31] A. D. Schlipf, M. Scherer, and M. Haller, “SWISS grid Test for secondary control capability,” no. 1.1, pp. 1–8, 2011.
- [32] J. Aho, A. Buckspan, and J. H. Laks, “A tutorial of wind turbine control for supporting grid frequency through active power control,” *Proc. Am. Control Conf.*, no. March, pp. 3120–3131, 2012.
- [33] F. Iov and L. Petersen, “Solar PV system performance model,” Smart Energy Systems Lab, Aalborg University, Aalborg, 2016.
- [34] D. Bertsimas and A. Thiele, “Robust and Data-Driven Optimization: Modern Decision Making Under Uncertainty,” *INFORMS Tutorials Oper. Res.*, vol. October, pp. 95–122, 2014.
- [35] H. T. C. Pedro and C. F. M. Coimbra, “Assessment of forecasting techniques for solar power production with no exogenous inputs,” *Sol. Energy*, vol. 86, no. 7, pp. 2017–2028, Jul. 2012.
- [36] P. Pinson, “Very-short-term probabilistic forecasting of wind power with generalized logit-normal distributions,” *J. R. Stat. Soc. Ser. C (Applied Stat.)*, vol. 61, no. 4, pp. 555–576, Aug. 2012.
- [37] A. D. Hansen, M. Altin, and N. A. Cutululis, “Modelling of wind power plant controller, wind speed time series, aggregation and sample results.” DTU Wind Energy E-0080, Roskilde, 2015.
- [38] [https://www.swissgrid.ch/dam/swissgrid/experts/ancillary\\_services/prequalification/D130422\\_Test-for-secondary-control-capability\\_V2R1\\_EN.pdf](https://www.swissgrid.ch/dam/swissgrid/experts/ancillary_services/prequalification/D130422_Test-for-secondary-control-capability_V2R1_EN.pdf)

- [39] Hansen A.D., Margaris I.D., Tarnowski G.C., Iov F., Kjær P.C., “Analysis of the short-term overproduction capability of variable speed wind turbines”, Renewable Energy Journal 68 (2014) 326-336
- [40] Impact of advanced wind power ancillary services on power system, DTU Wind Energy E-0081, ISBN 978-87-93278-26-4
- [41] J. C. Kuhlmann, Master Project Report, “Coordination of wind power plants for frequency control support,” DTU Wind Energy M-0139, June 2017.